NTNU
Norwegian University of
Science and Technology

Ceramic Thermal Barrier Coatings of Yttria Stabilized Zirconia Made by Spray Pyrolysis

Inga Askestad

Chemical Engineering and Biotechnology
Submission date: June 2011
Supervisor: Hilde Lea Lein, IMTE
Co-supervisor: Mari-Ann Einarsrud, IMT
Tor Grande, IMT
Sophie Weber, IMT

Norwegian University of Science and Technology
Department of Materials Science and Engineering

Preface

This master thesis was written as part of the course TMT 4900 at the Department of Materials Science and Engineering at the Norwegian University of Science and Technology (NTNU).

First of all I would like to thank my main supervisor Associate Professor Hilde Lea Lein and my co-supervisors PhD-candidate Sophie Weber, Professor Mari-Ann Einarsrud and Professor Tor Grande for guidance and support. Weber has also been absolutely great helping me with the lab work including e.g. sample preparation methods, and thermogravimetric analysis of coatings and powder. For help with the lab work and training I also want to thank Julian Tolchard and Gunn Torill Wikdahl.

I would like to thank the Inorganic Materials and Ceramic Research group at NTNU for the opportunity to get an insight in the research within the field of inorganic materials and the work performed by other master students and PhD-candidates. The weekly meetings with the ceramic group have given me helpful feedback, interesting discussions and a personal confidence in performing presentations.

Declaration

I hereby declare that the work in this master thesis is performed independently and in compliance with the regulations at NTNU.

Trondheim, 23.06.2011

_____

Inga Askestad

Abstract

A thermal barrier coating (TBC) is used as thermal protection of metallic components exposed to hot gas streams in e.g. gas turbine engines. Due to a high thermal expansion coefficient, low thermal conductivity, chemical- and thermal stability, yttria stabilized zirconia (YSZ) is the most widely used material for TBCs today.

In the work presented in this master thesis an aqueous nitrate precursor solution was prepared and deposited on stainless steel substrates by spray pyrolysis to produce 8YSZ coatings (8 mol% of Y_2O_3 in ZrO_2). The precursor solution concentration and deposition parameters, including set-point temperature and volume sprayed, were optimized to produce continuous and crack-free green coatings.

The deposited green coatings were characterized by scanning electron microscopy, thermogravimetry and Fourier transform infrared spectroscopy to study the influence of substrate temperature on the microstructure of the green coatings. A substantial change in microstructure was observed for the green coatings in a certain temperature range indicating that a minimum deposition temperature was necessary to obtain crack-free green coatings.

Heat treatment was necessary to decompose the nitrate species in the deposited film. During heat treatment, vertical cracks were introduced into the coatings due to the nitrate decomposition. The cracking behavior of the coatings was studied for different drying times and conditions, and it was found that the crack propagation can be controlled to obtain the preferred size and geometry of the cracks.

Due to built-up stresses in the coating, which can exceed the fracture toughness of the material, it was found that there was a maximum film thickness achievable before spallation of the coating for a given precursor solution. Therefore, the possibility of spraying multi-layered coatings was investigated. The introduction of a second layer showed that it was possible to double the thickness of the coating.

Table of Contents

Abbreviations

Abbreviation	Description
APS	Air Plasma Spray
c	Cubic
EBPVD	Electron Beam Physical Vapor Deposition
EDS	Energy Dispersive X-ray Spectroscopy
FTIR	Fourier Transform Infrared
g	Gram
LCZ	LZ doped with CeO_2
LZ	Lanthanum Zirconate
M	Concentration - mol/L
m	Monoclinic
Mol%	Mol percent
NTNU	Norwegian University of Science and Technology
SEM	Scanning Electron Microscope
SPPS	Solution Precursor Plasma Spray
t	Tetragonal
TBC	Thermal Barrier Coating
TGA	Thermogravimetric Analysis
TGO	Thermally Grown Oxide
Wt%	Weight percent
XRD	X-ray Diffraction
YSZ	Yttria Stabilized Zirconia

1 Introduction

Thermal barrier coatings (TBCs) are used to protect and insulate primarily metallic components when they are exposed to high temperatures. TBCs are used in a large extent to protect components from hot gas streams in e.g. gas turbine engines. A TBC normally consists of a base material called the substrate, a bond coat and a top coat. A bond coat is used to increase the high temperature oxidation resistance of the substrate and the adherence between the substrate and the top coat. The top coat is the insulation layer and should have a high wear resistance, good chemical and thermal stability and good heat insulating properties. During operation, a thermally grown oxide layer forms at the interface between the bond coat and the top coat. [1-3]

There are several basic requirements for a material to be used as a TBC: low thermal conductivity, high melting point, high thermal expansion coefficient, no phase transformation between room temperature and the operating temperature, low sintering rate, chemical inertness, high hardness and good adhesion to the substrate. With a high thermal expansion coefficient, low thermal conductivity, chemical- and thermal stability, yttria stabilized zirconia (YSZ) is the most widely used material for TBCs today. However, this material has a limiting operation temperature due to sintering and phase transitions at elevated temperatures. Next generation TBCs will result in increased temperature exposures of the top coat and new materials may therefore be required. Lanthanum zirconate (LZ) was recently proposed as a TBC candidate due to its promising properties: low sintering at high temperatures, no phase transitions, thermal and chemical stability, low thermal conductivity and no oxygen transparency. The drawback with LZ is the thermal expansion mismatch with the bond coat leading to spallation during temperature cycling. [4]

Studies have been carried out to increase the efficiency of gas turbine engines by increasing temperature and pressure during operation. This has been achieved by a combination of the right material selection, proper cooling systems and TBCs. Recent emphasis has been given to improve both economical and environmental aspects of the gas turbine engine. Commercial deposition techniques for TBCs, such as air plasma spraying (APS) and electron beam physical vapor deposition (EBPVD), are complex and expensive. As a consequence, spray pyrolysis, due to its simplicity, low costs and wet solution route, is a promising technique to deposit TBCs. [1-3]

In previous work by the author [5], spray pyrolysis was used to deposit LZ coatings on stainless steel from an aqueous nitrate precursor solution. Four different thick crack-free green coatings were prepared with different spray pyrolysis parameters. During heat treatment a continuous network of cracks were observed in the coatings, due to decomposition of the nitrate species remaining in the green coating.

Vertical cracks have been shown to be beneficial in TBCs because they can increase the coatings ability to tolerate thermal stress caused by thermal cycling and hence improve the coating

durability [6-7]. However, for TBC applications it is important that narrow vertical cracks are grown in a controlled manner [8]. Weber et al. [8] studied the deposition mechanisms of thick LZ coatings. Weber states that for TBCs made by spray pyrolysis of an aqueous nitrate precursor solution the vertical cracks should not be introduced into the coating during deposition, but rather during the decomposition of the nitrates after spray pyrolysis.

The aim of this master thesis was to prepare 8YSZ (8 mol% of Y_2O_3 in ZrO_2) coatings on stainless steel substrates by spray pyrolysis of an aqueous nitrate precursor solution. By lowering the amount of nitrate groups per cation in the precursor solutions from LZ to 8YSZ, the cracking behavior of the 8YSZ coatings was investigated. Deposition parameters were optimized for 8YSZ according to deposition mechanism to produce successful coatings, which were further characterized with regards to composition, microstructure and thickness.

2 Theoretical Presentation

2.1 Thermal Barrier Coatings

The purpose of using a TBC is to reduce the surface temperature of a base material (usually a metal) which is exposed to high temperatures. Birks et al. [9] states that it is possible to achieve a temperature decrease on the metal surface of about 175 ˚C when using a suitable TBC. A temperature drop on the metal component surface will delay failure caused by oxidation or high temperature corrosion of the base material or thermally induced failure mechanisms such as thermal fatigue [10]. Finally, TBCs allow the possibility to perform at temperatures above the melting temperature of the metal.

TBCs are thermally insulating materials which must sustain a substantial temperature difference between the base material and the coating surface. Because of a high wear resistance, good chemical and thermal stability together with good heat isolating properties, ceramic materials are proper materials for TBCs. [3]

The structure of a TBC is quite complex as shown in the example in Figure 2.1. It typically consists of four layers: the metal substrate, a bond-coat, a thermally grown oxide (TGO) layer and a ceramic top-coat, all having different physical, thermal and mechanical properties. [1]

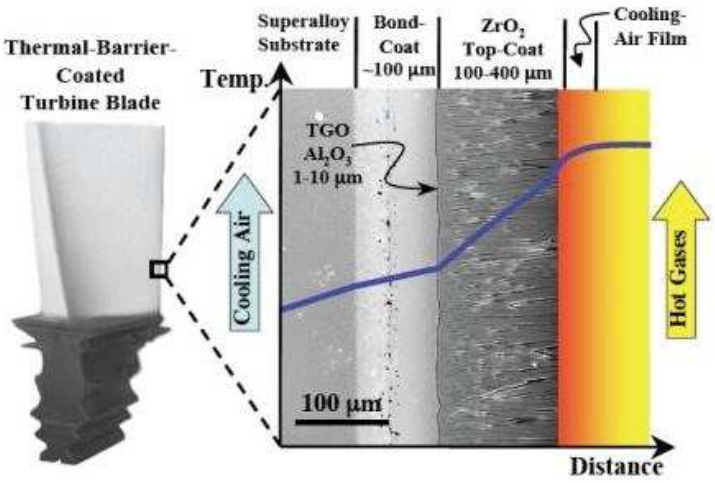

Figure 2.1: An example of the structure of a thermal barrier coated turbine blade. [11]

The substrate is the base material of the component. The substrate is usually a superalloy, but TBCs have also been introduced on composite materials [12]. The substrate is cooled with air from the inside or through air channels in the substrate to remove the heat conducted through the TBC. Even though the substrate is being protected with a TBC, the temperature on the surface remains high. The substrate therefore needs to withstand high temperature and be corrosion resistant at the temperature it is directly exposed to. [1]

On top of the substrate, an oxidation and hot corrosion resistant metallic layer, defined as the bond coat, is often applied. The main purpose of this layer is to increase the high temperature oxidation resistance of the substrate and to increase the adherence between the substrate and the top coat. An ideal bond coat should have a thermal expansion coefficient that matches thermal expansion coefficients of both the superalloy and the ceramic top coat. It is also important that the bond coat adhere to the substrate with minimum stresses and remains stable during long term high temperature exposure and thermal cycling [1]. Because of the porosity in the ceramic top coat, oxygen is able to diffuse through the top coat and down to the surface of the bond coat leading to oxidation of the bond coat at high temperatures. The oxidation of the bond coat leads to the formation of a TGO film. Aluminium enriched materials are preferable to use as bond coats because the oxidation of aluminium creates a slow growing and adherent alumina film at the interface which slows down the oxidation process. This oxide also has one of the lowest oxygen diffusion rates of all protective oxide films, and hence gives good protection of the underlying metal. [2, 10]

A typical TBC usually refers to both the bond coat and the ceramic top layer. However, in this report, the ceramic top coat by itself is referred to as the TBC.

2.2 Area of Application

The most widely use of TBCs is in gas turbine engines to protect the different metallic components from the hot gas stream. The gas turbine engine was invented in the mid 1900s and today gas turbines are used for aircraft or marine propulsion or are land based for power generation. [9]

A schematic overview of a gas turbine engine is shown in Figure 2.2a. It consists of three main parts [13]:

- A compressor where air is sucked in by the compressor and compressed to a high pressure.
- A combustion area where fuel (e.g. propane or natural gas) is mixed with air coming from the compressor. The mixture is then ignited so that the fuel burns and produces gas with high pressure and high velocity.
- A turbine section where the pressurized gas from the combustion area spins the turbine which transforms the kinetic energy of the gas to rotary energy. This rotary energy is a great energy source which can e.g. drive a generator transforming the mechanical energy from the turbine to electrical energy.

TBCs are used to insulate the metallic surfaces of components in the combustor and turbine section, especially on parts exposed to the highest temperatures such as the initial rotor blades (turbine blades), the combustor and the nozzle guide vanes of the turbine. Figure 2.2b shows the pressure and temperature profile along a jet engine. [2]

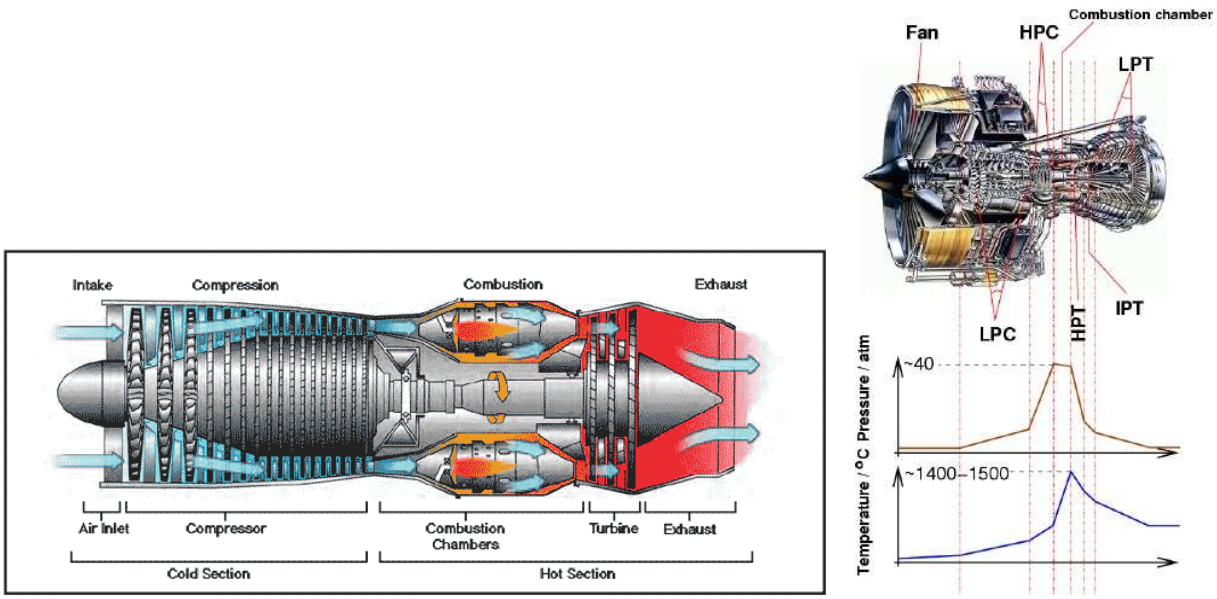

a) b)

Figure 2.2: a) A schematic overview of a gas turbine engine. **b**) Pressure and temperature profiles along a jet engine. [14]

During the past 30 years great efforts have been made to achieve a higher efficiency (reduced fuel consumption and higher power output) of a gas turbine engine. A combination of material improvements including use of TBCs and improved methods for internal and external cooling have made it possible to increase the temperature and pressure in the gas turbine engine. [3]

Research on TBCs is done both of economical and environmental aspects. When the operating temperature of an engine can be increased the thermodynamic efficiency is improved and the pollutant emission is reduced. [14]

2.3 Degradation of TBCs

One of the biggest concerns for TBCs is the coating durability and particularly the premature spallation failure of the coating during service. Spallation leads to direct contact between the substrate and the hot corrosive environment. [1]

The main causes of premature spallation failure are [1-2]:

- Thermal expansion mismatch between the substrate and the ceramic material causing stresses.
- The continuously change of properties, compositions, microstructure and interfacial morphology throughout the TBC system.
- Oxidation of the metal substrate.
- Growth of TGO during operation. TGO growth creates a volume expansion leading to out of plane compressive stresses in the top coat which can result in initiation and propagation of cracks.

Sintering of the ceramic top coat might happen during high temperature exposure. Sintering leads to an increase in thermal conductivity, but can also contribute to increased elastic strain energy stored in the TBC which can enhance the driving force for spallation. [9]

2.4 Thermal Properties

2.4.1 Thermal Conductivity

Thermal conductivity is equivalent to the heat flow through a material. The thermal conductivity (λ) of a material is proportional to heat capacity (c_p), the quantity and velocity of heat carriers (v) and the mean free path of the heat carriers (m) as described in Equation 1:

$$\lambda \propto c_p v m \tag{1}$$

In metals the electrons are the heat carriers. Metals contain a large amount of electrons which are relatively free to move throughout the material giving high thermal conductivity. In ceramics, however, thermal energy is carried by phonons or radiation through pores. [3]

Porosity in a ceramic material decreases the thermal conductivity because air is a poor heat conductor. When sintered, a ceramic component will densify and the particles will coarsen leading to a decrease in pore density. Sintering therefore leads to a higher thermal conductivity which is unwanted for TBCs. [3]

2.4.2 Thermal Expansion

Thermal expansion refers to the change in dimensions that occurs with most materials as the temperature is increased or decreased. The degree of dimensional change depends on the strength of the atomic bonding together with the arrangement of atoms in the material. Metals often have a closed pack structure and relatively weak bonding between atoms which gives metals a high thermal expansion coefficient. For ceramic materials the thermal expansion depends on the degree of ionic and covalent bonding. It is important that the TBC has a thermal expansion which matches the metal substrate in order to avoid coating degradation during thermal cycling. [3]

2.5 Material Selection

The earliest TBCs were frit enamels applied to aircraft engine components in the 1950s. The first ceramic TBCs were made of alumina and MgO/CaO stabilized zirconia applied by plasma spraying. [9]

Al_2O_3, TiO_2, CaO/MgO + ZrO_2, CeO_2, YSZ, $La_2Zr_2O_3$, mullite, rare earth oxides and metal-glass composites, all described by CaO et al. [4] in a review about TBC materials, have been investigated as TBCs.

2.5.1 Material Requirements for TBCs

To improve the heat insulation of a TBC, the ceramic coating should have tailored microstructure and pore structure and both thermal and chemical stability in different atmospheres. Table 2.1 lists some basic material requirements for the ceramic top coat material. The thermal expansion coefficient and the thermal conductivity have proved to be the most important material properties when selecting a proper ceramic material for a TBC. [4]

Table 2.1: Material requirements for a ceramic TBC. [4, 15]

Requirement	**Explanation**
Low thermal conductivity	To thermally insulate the superalloy component.
High melting point	To be able to operate in the high temperature environment in a gas turbine engine.
High thermal expansion coefficient	To match the thermal expansion coefficient of the underlying superalloy to decrease stresses at the interface.
No phase transformation between room and operating temperature	A phase change during thermal cycling can be structurally detrimental.
Low sintering rate of the porous structure of the coating	To avoid pore elimination leading to an increase in thermal conductivity.
Chemical inertness	To be oxidation and corrosion resistant in the operating environment.
High hardness and good adhesion to the substrate	To protect the component from erosion and wear.

So far, no single material has been found to satisfy all the material requirements listed above. Commercial TBCs are currently made of YSZ, however LZ has shown promising properties. [5]

2.5.2 Yttria Stabilized Zirconia

YSZ has the general formula $Zr_{1-x}Y_xO_{2-x/2}$ and is the most widely used material for TBCs today. YSZ has shown the best performances in high temperature applications such as diesel engines and gas turbine engines. YSZ is preferred due to its excellent properties [1, 4]:

- YSZ has a thermal conductivity of around 2.3 W/mK at 1000 °C for a fully dense material, and it is therefore among the ceramic materials with the lowest thermal conductivity at high temperatures. The low thermal conductivity is mainly caused by its high concentration of point defects, which scatters the phonons.
- YSZ has a high thermal expansion coefficient of around $11 \cdot 10^{-6}$ $°C^{-1}$, only slightly lower than the one for the metallic substrates ($\sim 14 \cdot 10^{-6}$ $°C^{-1}$).
- The low density of YSZ is an advantage because the coating will not dramatically increase the weight of the component.

- YSZ has a high hardness (~14 GPa), which is beneficial regarding wear and erosion.
- YSZ is resistant to ambient and hot corrosion.
- YSZ has a high melting point.

The crystal structure of pure ZrO_2 changes with temperature, a phenomenon called polymorphism. As shown in the phase diagram in Figure 2.3, pure ZrO_2 has a monoclinic (m) crystal structure from ambient temperature up to around 1170 °C where it transforms into a tetragonal (t) phase and further to a cubic (c) phase at about 2370 °C. The cubic phase is stable up to the melting point of about 2700 °C. [16]

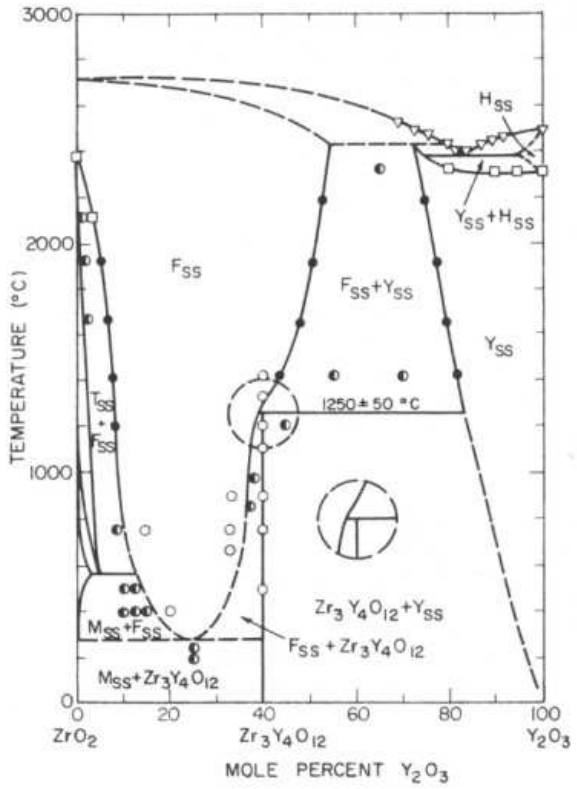

Figure 2.3: Phase diagram of the ZrO_2-Y_2O_3 system. [17]

The different polymorphs of zirconia have structures which are closely related to the fluorite structure shown in Figure 2.4. The fluorite structure originates from the naturally occurring fluorite mineral CaF_2. The cations lie in an expanded face centered cubic structure. The anions occupy all the tetrahedral sites and are therefore surrounded by four cations. The cations are surrounded by a cubic array of eight anions. [18]

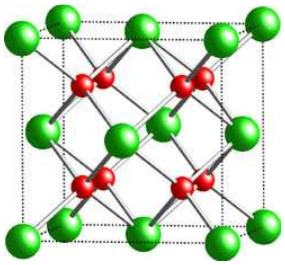

Figure 2.4: The fluorite structure, CaF_2 (green: Ca^{2+}, red: F^-). [19]

The monoclinic crystal structure of zirconia (baddeleiyte) is a distortion of the fluorite structure where zirconium is surrounded by an irregular polyhedral of only seven oxygen ions [20]. The phase transition from monoclinic to tetragonal is caused by the polyhedral becoming more regular and zirconium being surrounded by eight oxygen ions [21]. The tetragonal structure is like the fluorite structure except that the oxygen ions are slightly displaced from the ideal fluorite position [21]. The cubic crystal structure of zirconia has the fluorite structure where zirconium is surrounded by eight oxygen ions at the corners of a cube [22].

The phase transformation between m-ZrO_2 and t-ZrO_2 occurs at around 1170 °C. The transformation from t-ZrO_2 to m-ZrO_2, however, occurs around 970 °C. This is a martensitic phase transition because it only occurs by displacements of atoms in the structure and it does not require diffusion. This martensitic phase transition involves a significant volume change of 3-5 %, which will induce a significant shear strain and cause cracking and weakness in the ceramic coating. [15, 22]

To avoid the phase transformation from m to t during high temperature exposure, it is possible to stabilize at room temperature the high temperature tetragonal and cubic phases of zirconia by aliovalent substitution of lower valent oxides such as CaO, MgO or Y_2O_3. Stabilization of the high temperature phases will further eliminate the undesirable volume change. [4, 12]

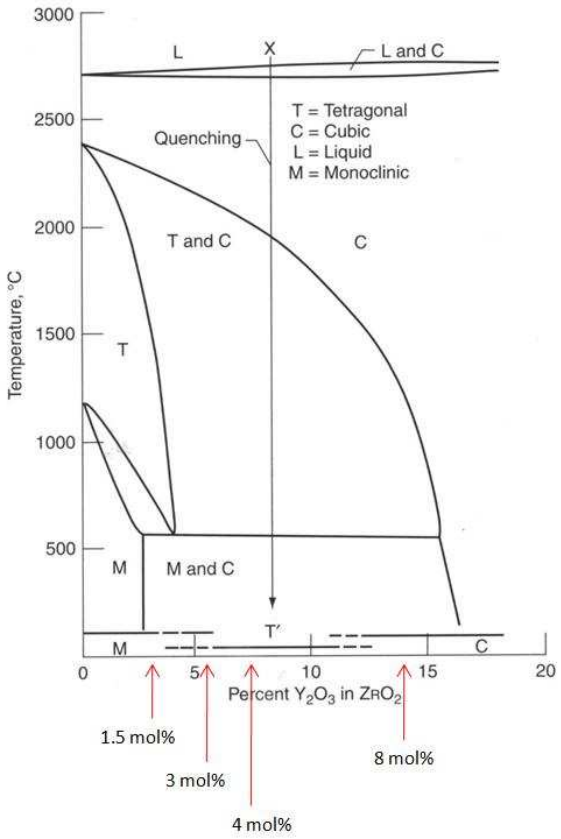

Figure 2.5: The zirconia rich part of the phase diagram of the ZrO_2-Y_2O_3 system. The unit of the x-axis is wt% Y_2O_3 in ZrO_2. The horizontal lines in the bottom of the diagram, designated by m, t' and c, indicate the different metastable phases.

Figure 2.5 shows the zirconia rich part of the phase diagram of the ZrO_2-Y_2O_3 system. During deposition of a TBC by conventional methods, the deposited structures rarely achieve equilibrium due to the very rapid cooling of the molten particles. In the phase diagram in Figure 2.5, the formation of metastable phases are included by three discontinuous horizontal lines identified as m, t’ and c. It can be seen from the phase diagram that an yttria content of less than around 4 wt% (~2.2 mol%) will give the martensitic transformation from t to m during cooling from high temperatures. For an yttria content in the range 4-11 wt% (2.2-6.3 mol%) the c-phase will, if rapidly cooled, transform to a non-transformable t-phase called t’, which remains stable at room temperature. The t’ is crystallographically the same as the t phase. For yttrium contents higher than 11 wt%, the c-phase is stabilized down to room temperature. [15]

Zhou et al. [23] deposited TBCs of 8 wt% yttria partially stabilized zirconia by APS on titanium substrates. Even though the feedstock material contained the tetragonal, cubic and monoclinic phases, the ceramic coating did only contain the metastable tetragonal t’-phase. However, the t’-phase will, during high temperature cycles, transform to t-phase and c-phase and the tetragonal t-phase will further transform to the m-phase. [23]

High temperature durability rig testing at NASA showed that the optimum yttria content was around 7 wt% (equivalent to about 4 mol%). This yttria content will stabilize the t'-phase at room temperature. Significantly lower contents of yttria will not inhibit the transformation from t to m, and significantly higher contents will stabilize the cubic phase, which lacks the strength and durability of the t' phase. [15]

One of the disadvantages of YSZ is the oxygen transparency. The stabilization of ZrO_2 with Y_2O_3 occurs according to Equation 2:

$$2\mathrm{ZrO}_2 \overset{\mathrm{Y_2O_3}}{\rightarrow} 2Y'_{Zr} + V_O^{\cdot\cdot} + 3O_o^x \qquad (2)$$

As shown by the equation, YSZ includes oxygen vacancies. The number of vacancies increases as the temperature increases leading to oxygen transparency at high temperatures causing corrosion or oxidation of the underlying metallic layer. [16]

Another disadvantage of YSZ for TBC application is the limiting operation temperature (< 1200 °C) due to sintering and a phase transition, which occurs during high temperature exposure. The material transforms from the metastable t'-phase to the equilibrium t- and c-phase and back to the monoclinic phase at room temperature during thermal cycling. [4]

The phase transformation from t to m was shown to be hindered by the doping of YSZ by CeO_2. In addition, CeO_2 has a higher thermal expansion coefficient than YSZ leading to an increase of thermal expansion coefficient in the doped YSZ. However, the effects of the doping on the hardness properties and the sintering rate were detrimental. [4]

ZrO_2 stabilized by CaO or MgO has also been studied, but they show less corrosion resistance against compounds such as Na_2SO_4. According to the literature CaO and MgO stabilized ZrO_2 has an operation temperature limit of 927 °C. Another disadvantage with these materials is that when substituting Y^{4+} with Ca^{2+} two oxygen vacancies forms. Therefore, the coatings include a great amount of oxygen ion vacancies, which leads to oxygen transport to the bond coat at high temperatures causing the formation of a TGO layer which might lead to spallation if the bond coat is not oxidation resistant. [4]

2.5.3 Lanthanum Zirconate - $La_2Zr_2O_7$

LZ was recently proposed as a promising TBC material, due to its high thermal stability, low thermal conductivity, low sintering at high temperatures and because it is not oxygen transparent. [4]

LZ has a cubic pyrochlore structure, stable up to its melting temperature, and it is referred to as a rare-earth pyrochlore with general formula $Re_2Zr_2O_7$ (Re=rare earth). The pyrochlore structure consists of corner-shared ZrO_6 octahedra forming the back bone of the network as shown in Figure 2.6. La^{3+} fills the sites formed by six ZrO_6 octahedra. The thermal properties of this

material can be tailored by substituting La^{3+} and Zr^{4+} with other elements with similar ionic radii. [4, 24-25]

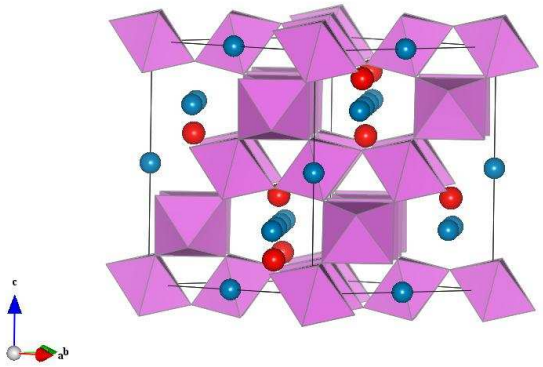

Figure 2.6: Structure of LZ (blue: lanthanum, red: oxygen, violet octahedrons: zirconium surrounded by six oxygen atoms). The figure was made with the software VESTA, using data from Springer Materials [26].

The drawback with LZ is the low thermal expansion coefficient compared to the metallic substrate. However, the thermal expansion coefficient can be increased by doping. Zhou et al. [27] investigated the possibility of doping LZ with CeO_2 (LCZ) to increase the thermal expansion coefficient. Results showed an increase in the thermal expansion coefficient and a decrease in thermal conductivity compared to LZ and 8 wt% YSZ.

In a project work [5] performed by the author in 2010, porous coatings of LZ were prepared on stainless steel substrates by spray pyrolysis. A mixture of aqueous lanthanum and zirconyl nitrate solutions was used as the precursor solution and four different coatings were prepared with varying spray pyrolysis parameters. The coatings were further characterized with regards to composition, microstructure, coating thickness and roughness, hardness, thermal properties and thermal stability. The thicknesses of the coatings were found to be in the range of 45-115 µm. The fine and porous microstructure of the coatings made them suitable as TBCs (Figure 2.7 a). This was verified by measurements of thermal diffusivity and conductivity of one of the four coatings by the Laser Flash method. Measurements showed that the thermal conductivity decreased with increasing temperature to a minimum of 0.2 W/mK at 300 °C before it increased again. During heat treatment of the coatings, cracks were observed over the whole surface as shown in Figure 2.7b and c. The cracking of the coatings was found to be caused by the decomposition of the nitrate precursor solution which generated tensile stresses in the coatings during heat treatment after spray pyrolysis.

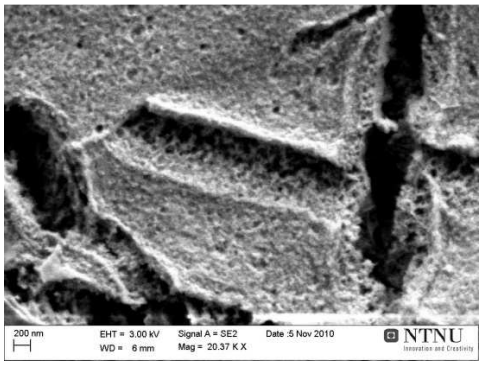

a)

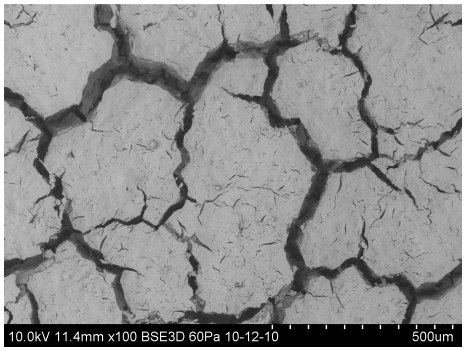

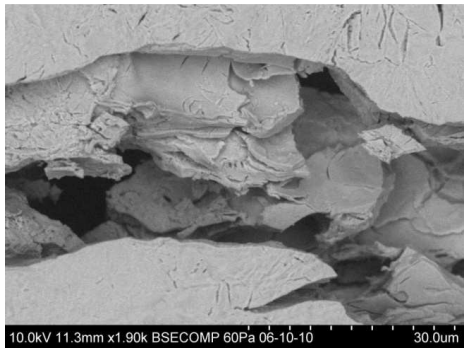

b) c)

Figure 2.7: Figure **a** shows porosity in LZ coatings which contributed to the low thermal conductivity. Figure **b** and **c** shows cracks caused by the decomposition of the nitrates during heat treatment. [5]

2.6 Deposition Techniques

2.6.1 EBPVD, APS and SPPS

TBCs are currently deposited by APS or EBPVD. EBPVD is a preferred method for components which require to withstand a high degree of thermo-mechanical strain due to the fine columnar microstructure, whereas APS produces “splat” grain morphology, which is commonly used to obtain minimal thermal conductivity. [2]

In APS, a plasma jet (a collection of charged and neutral particles formed by ionization of a gas) melts the coating raw material in the form of powder. A high pressure gas transports the molten particles to the substrate where it cools and forms a coating. EBPVD is a technique where one makes use of the high power of a focused electron beam, which melts and vaporizes the sintered cylindrical ingots of the raw feedstock material. The substrate to be coated is then positioned above the melted pool and molecules in the vapor are deposited on the substrate surface. [15]

Both EBPVD and APS use powders as a feedstock material, whereas liquid solutions as raw material offer simplicity and improved control of the coating composition. Solution precursor plasma spray (SPPS) was recently developed in order to take advantage of the liquid precursor solution. In a process similar to APS, the raw liquid material is fed to the plasma as atomized

droplets of a precursor solution, to deposit a coating with similar performances to the coatings made by APS. [6]

2.6.2 Spray Pyrolysis

Compared to EBPVD, APS and SPPS spray pyrolysis is a simple and easy technique which does not require complex equipments or vacuum. Due to its simplicity it is also a cost effective method, especially regarding equipment costs. In spray pyrolysis the precursor solution is transported towards the substrate as an aerosol. The method is used to produce thin or thick, single or multilayered coatings on a substrate. The method is schematically illustrated in Figure 2.8. The method is currently used to deposit thin films for applications such as solar cells or oxide fuel cells, but attention has also been placed to understand the mechanisms occurring during deposition. [28]

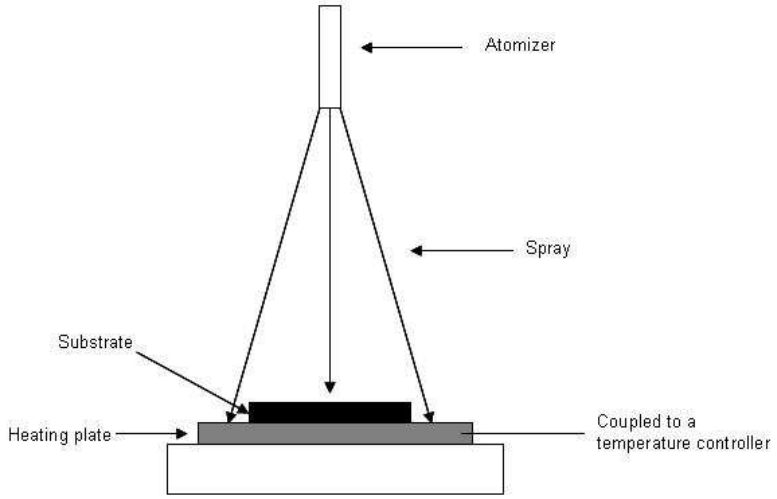

Figure 2.8: A schematic illustration of the spray pyrolysis method.

The properties and structure of the deposited film have shown to be highly dependent on the spray pyrolysis parameters such as:

- Type and concentration of precursor solution
- Substrate temperature
- Spraying distance
- Flow rate of precursor solution
- Volume of precursor solution
- Carrier gas pressure

The type of nozzle, carrier gas and carrier gas pressure will determine the droplet size distribution whereas the precursor solution chemistry such as solubility, density and solvent boiling point will influence the evolution of the droplets during the transport to the substrate. Several studies describe temperature as the most important spray pyrolysis parameter.

Changing the temperature will influence the film formation and directly change the properties and morphology of the film. [8, 28]

Perednis et al. [28] have divided the deposition of thin films using spray pyrolysis into three main steps: atomization of precursor solution, aerosol transport and decomposition of precursor on the substrate. The aerosol transport and the decomposition of precursor are highly temperature dependent. When aerosol droplets are transported to the substrate, some or all of the solvent evaporates due to the high temperature in the air above the heating plate. However, it is desirable that as many droplets as possible reach the substrate without forming powder particles during transport. Indeed, when a droplet hits the substrate, many processes occur such as evaporation of the remaining solvent, spreading of the droplet and decomposition of ionic salt. Perednis et al. investigated the influence of the temperature and spraying distance in the state of the precursor solution during transport. They proposed a deposition mechanism similar to the chemical vapor deposition process.

Weber et al. [8] investigated the deposition of LZ coatings by spray pyrolysis on stainless steel substrates. Through this study Weber describes the influence of the film formation mechanisms, deposition temperature and salt decomposition on the coating composition and microstructure. Weber also proposed a deposition mechanism of thick films made by spray pyrolysis from aqueous nitrate precursor solutions. The mechanism is graphically illustrated as a function of substrate temperature in Figure 2.9.

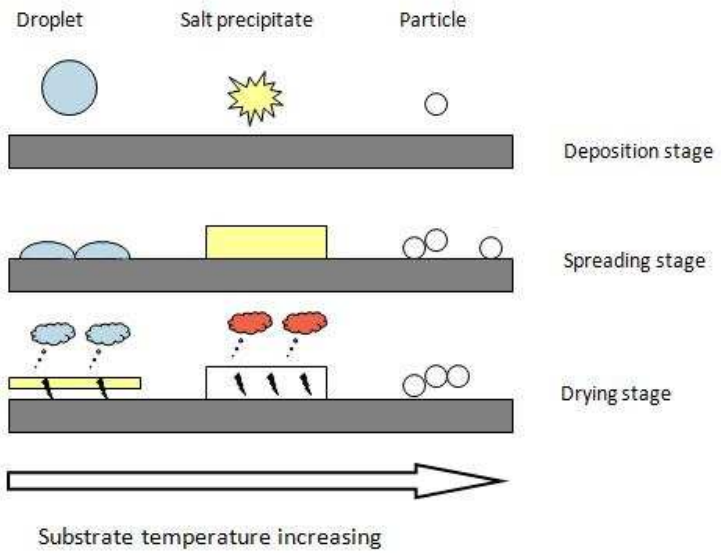

Figure 2.9: Schematic description of the deposition and film formation mechanism with increasing substrate temperature. [8]

Weber found that the deposition of continuous crack-free green thick films of LZ from nitrate solutions was only possible in a specific temperature interval. Below a minimum deposition temperature, wet droplets hit the substrate and the solvent is therefore still present in the

deposited film. This will generate stresses in the coating due to a large amount of products to evaporate and decompose further resulting in cracks and delamination. Above a maximum deposition temperature the solvent evaporates from the droplets and an ionic salt precipitate is formed. The ionic salt decomposes further during spraying and spreading on the substrate. If the decomposition is completed during spraying, oxide particles will hit the substrate. In addition the air stream being directed parallel to the substrate surface flowing outwards will carry away the lighter oxide particles, resulting in the deposition of a thin film of weakly bonded oxide particles. Moreover, if the decomposition is completed during spreading on the substrate, the impacted material does not bond with the already deposited material creating irregular deposits on the substrate. [8]

At an intermediate temperature, the solvent will evaporate during transport towards the substrate and the resulting ionic salt precipitate is deposited and spread to form a coating. The partial decomposition of nitrate salts starts at the latest stage of the deposition without introducing cracks, producing a crack-free green coating. Variations of the temperature within the temperature interval suitable for crack-free green coatings will also affect the microstructure and further treatment of the coatings. [8]

3 Experimental Work

3.1 Preparation of Precursor Solution

The chemicals used to prepare the precursor solution are listed in Table 3.1.

Table 3.1: Chemicals used to prepare the precursor solution.

Chemical	Formula	Supplier	CAS
Yttrium (III) nitrate hexahydrate (99.8 %)	$Y(NO_3)_3{\cdot}6H_2O$	Aldrich	13494-98-9
Zirconyl (IV) oxynitrate hydrate (99.0 %)	$ZrO(NO_3)_2 \cdot xH_2O$	Aldrich	14985-18-3

Aqueous solutions of $Y(NO_3)_3{\cdot}6H_2O$ (0.5 mol/L) and $ZrO(NO_3)_2{\cdot}xH_2O$ (0.5 mol/L) were prepared and thermogravimetrically standardized to find the exact concentration, due to the uncertainty caused by crystal water. The temperature program used for the standardization is shown in Figure 3.1. The weight of the nitrates and the resulting oxides was measured and used to calculate the cation concentration in the aqueous solutions. The precursor solution was then prepared by stoichiometrically mixing the two solutions and concentration was adjusted by dilution when required.

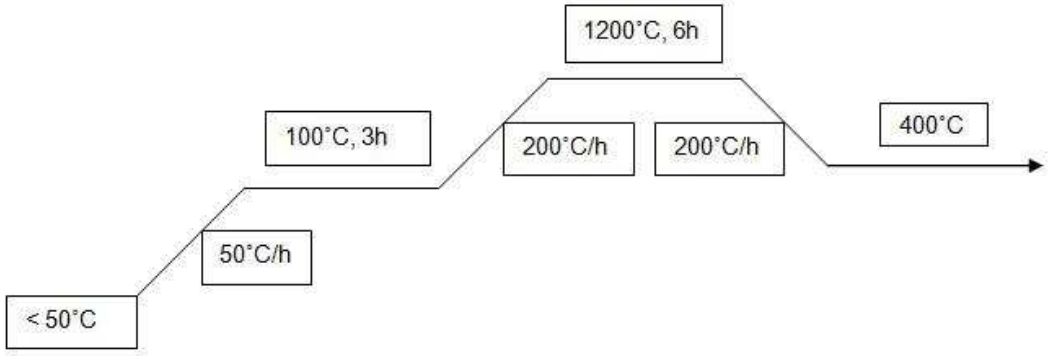

Figure 3.1: Temperature program for thermogravimetric standardization of the two nitrate solutions.

3.2 Substrate Preparation

The precursor solution was used to coat stainless steel substrates by use of spray pyrolysis. AISI 304 was chosen as the substrate material in this work. AISI 304 is an austenitic nickel-chromium based alloy (18-20 % Cr and 8-10.5 % Ni) [29]. The stainless steel substrates with a thickness of 0.5 mm were cut into two different geometries, either quadratic (2.5 cm * 3 cm) or circular (diameter of 2.5 cm), and then cleaned with ethanol.

3.3 Powder Characterization

To check the stoichiometry of the precursor solution, x-ray diffraction (XRD) measurements were performed on powder made from precursor solutions with different compositions. Precursor solutions with molar ratios of 3:97, 6:94, 8:92 and 16:84 of Y to Zr were heated to

150 °C for 15 hours to evaporate the water. Each powder was crushed to small particles with a mortar before it was pressed to a pellet. Powder pellets were calcined at 1100 °C for two hours with heating and cooling rates of 100 °C/h. The powder composition was determined using XRD (D8 Focus X-ray diffractometer) with Cu Kα radiation. A solution of powder and ethanol was put on a Si single crystal sample holder and dried for 5 minutes to evaporate ethanol.

3.4 Spray Pyrolysis – Coating Preparation

3.4.1 Spray Pyrolysis Apparatus

The spray pyrolysis apparatus used in this work has been designed and built at NTNU by PhD candidate Sophie Weber, and a schematic drawing of the apparatus is shown in Figure 3.2. The precursor solution was mixed with a synthetic carrier gas in the nozzle and sprayed onto a heated substrate as an aerosol. The substrate was heated up by a heating plate connected to a thermocouple controller. The spray unit could be moved vertically to change the spraying distance and the pump controlled the volume and flow rate of the precursor solution. The heating plate was made of AlN and it was covered with a thin steel plate during spraying as protection. [30]

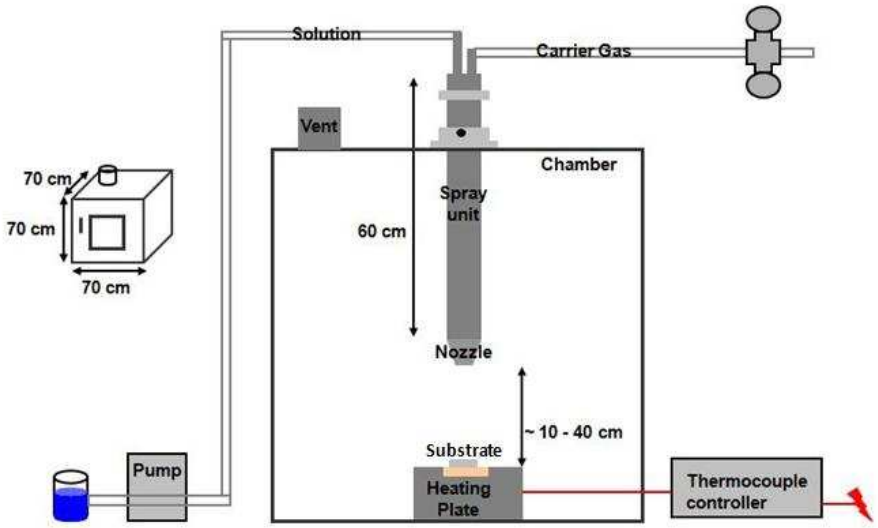

Figure 3.2: Spray pyrolysis apparatus used in this master thesis. [8]

At a given set-point temperature the substrate experienced different temperatures dependent on the spray pyrolysis conditions. The temperature on the heating plate, the temperature on the substrate with gas supply and the temperature on the substrate without gas supply have been measured at different set-point temperatures by Weber [30]. The measurements can be seen in Table 3.2. During spray pyrolysis both the gas and the liquid droplets cooled down the substrate. The temperature the substrate was exposed to during spray pyrolysis was therefore slightly lower than the substrate temperature with gas supply. The temperature the substrate

was exposed to during heat treatment or drying on the heating plate was either the substrate temperature with gas or the substrate temperature without gas depending on the drying conditions used for each coating.

Table 3.2: Temperature measurements for the heating plate and the substrate with and without gas supply at given set-point temperatures. [30]

Set-point temperature [˚C]	**Substrate temperature with gas supply [˚C]**	**Substrate temperature without gas supply [˚C]**	**Heating plate temperature [˚C]**
400	66	219	282
500	104	302	354
600	141	374	431
700	192	442	502
800	240	507	582
850	278	542	612
900	315	573	645

3.4.2 Coating Composition and Precursor Concentration

Coatings of 8YSZ (8 mol% Y_2O_3 in ZrO_2) were deposited by spray pyrolysis. The concentration of the precursor solution was varied according to Table 3.3 and is given in two different units. The exact concentration, shown in the second column, is given in $mol_{Zr4+}/g_{solution}$. The unit used for concentration in this master thesis, shown in the third column, is given in mol/L (M). The concentration of the precursor solution was adjusted by mixing the two nitrate solutions according to stoichiometry before the solution was further diluted.

Table 3.3: Different concentrations of the different precursor solutions.

Coating	**Concentration [$mol_{Zr4+}/g_{solution}$]**	**Concentration [mol/L]**
8YSZ	$2.62 \cdot 10^{-4}$	0.5
	$1.31 \cdot 10^{-4}$	0.25
	$0.655 \cdot 10^{-4}$	0.125

3.4.3 Spray Pyrolysis Parameters

To deposit continuous and crack-free green coatings suitable spray pyrolysis parameters had to be found. Based on previous experiments with the given spray pyrolysis method and apparatus [5], the air pressure (synthetic air) was set to 0.5 bar, the volume flow was set to 1 ml/min and the spraying distance was set to 25 cm. Depending on the concentration of the precursor solution, 10 or 20 ml were sprayed onto the substrate.

To determine which substrate temperature to use during spray pyrolysis, thermogravimetric analysis (TGA) was performed on 1.5YSZ, 3YSZ, 4YSZ and 8YSZ powders made from precursor

solutions with the same procedure as described in Section 3.3. A STA 449C apparatus from Netzsch was used to perform the experiments.

Five, ten and six different coatings were prepared using spray pyrolysis with respectively the 0.5, 0.25 and 0.125 M precursor solutions and the spray pyrolysis parameters shown in Table 3.4, Table 3.5 and Table 3.6.

The coating name 8YSZ(A)-B-C-D reflects the variations in concentration of precursor solution (A), set-point temperature (B), volume sprayed (C) and drying time and condition (D).

Table 3.4: Spray pyrolysis parameters for coatings prepared from the 0.5 M precursor solution. ND means that the coating was taken out of the apparatus immediately after the liquid flow stopped without drying on the heating plate.

No.	Coating name	Set-point temperature [°C]	Volume sprayed [ml]	Drying time [min]
1	8YSZ(0.5)-600-10-ND	600	10	0
2	8YSZ(0.5)-650-10-ND	650	10	0
3	8YSZ(0.5)-700-10-ND	700	10	0
4	8YSZ(0.5)-750-10-ND	750	10	0
5	8YSZ(0.5)-800-10-ND	800	10	0

Table 3.5: Spray pyrolysis parameters for coatings prepared from the 0.25 M precursor solution. ND means that the coating was taken out of the apparatus immediately after the liquid flow stopped without drying on the heating plate. $5min^{-}$ and $15min^{-}$ mean that the coating has been dried for 5 and 15 minutes without gas respectively.

No.	Coating name	Set-point temperature [°C]	Volume sprayed [ml]	Drying time [min]	Drying condition
6	8YSZ(0.25)-650-10-ND	650	10	0	
7	8YSZ(0.25)-675-10-ND	675	10	0	
8	8YSZ(0.25)-700-10-ND	700	10	0	
9	8YSZ(0.25)-700-10-$5min^{-}$	700	10	5	Without gas
10	8YSZ(0.25)-700-10-$15min^{-}$	700	10	15	Without gas
11	8YSZ(0.25)-700-20-ND	700	20	0	
12	8YSZ(0.25)-700-20-$15min^{-}$	700	20	15	Without gas
13	8YSZ(0.25)-700-5-ND	700	5	0	
14	8YSZ(0.25)-725-10-ND	725	10	0	
15	8YSZ(0.25)-750-10-ND	750	10	0	

Table 3.6: Spray pyrolysis parameters for coatings prepared from the 0.125 M precursor solution. ND means that the coating was taken out of the apparatus immediately after the liquid flow stopped without drying on the heating plate. $5min^{+}$, $5min^{-}$ and 15 min^{-} mean that the coating has been dried for 5 minutes with gas and 5 and 15 minutes without gas respectively.

No.	Coating name	Set-point temperature [°C]	Volume sprayed [ml]	Drying time [min]	Drying condition
16	8YSZ(0.125)-650-20-ND	650	20	0	
17	8YSZ(0.125)-700-20-ND	700	20	0	
18	8YSZ(0.125)-700-20-$5min^{+}$	700	20	5	With gas
19	8YSZ(0.125)-700-20-$5min^{-}$	700	20	5	Without gas
20	8YSZ(0.125)-700-20-$15min^{-}$	700	20	15	Without gas
21	8YSZ(0.125)-750-20-ND	750	20	0	

As shown in Table 3.4, Table 3.5 and Table 3.6 coatings were prepared with varying drying conditions. To have better control of the microstructure of the green coating after deposition some coatings were taken out of the spray pyrolysis apparatus immediately after the liquid flow stopped. To study the influence of heat treatment on the coatings some were dried with a high heating rate on the heating plate with or without gas while some were sprayed without drying on the heating plate and put into a high temperature furnace (600 °C) for slow heating (5 °C/h) instead. The coatings dried with slow heating rate are listed in Table 3.7.

Table 3.7: Coatings made from precursor solutions with concentration 0.25 M and 0.125 M sprayed at a set-point temperature of 700 °C with 10 and 20 ml respectively, where heat treated in a furnace to 600 °C for 2 hours with heating and cooling rates of 5 °C/h. SH means slow heating in a furnace.

No.	Coating name	Set-point temperature [°C]	Volume sprayed [ml]	Drying time and conditions
22	8YSZ(0.25)-700-10-SH	700	10	Heated to 600 °C for 2 hours with heating and cooling rates of 5 °C/h.
23	8YSZ(0.125)-700-20-SH	700	20	

3.4.4 Multi-Layered Coatings

Two different coatings were prepared with two layers on top of each other. The concentration of the precursor solution was 0.125 M and the spray pyrolysis parameters are shown in Table 3.8. The coating dried for 5 minutes with gas after each layer (coating 24) was exposed to a substrate temperature of 192 °C during drying. The coating dried for 5 minutes without gas after each layer (coating 25) was exposed to a substrate temperature of about 440 °C during drying.

Table 3.8: Spray pyrolysis parameters used for the two-layered coatings 8YSZ(0.125)-700-2x20-2x5min^{+} and 8YSZ(0.125)-700-2x20-2x5min^{-}.

			Layer 1 and 2		
Coating no.	**Coating name**	**Set-point temperature [°C]**	**Volume sprayed [ml]**	**Drying time [min]**	**Drying conditions**
24	8YSZ(0.125)-700-2x20-2x5min^{+}	700	20	5	With gas
25	8YSZ(0.125)-700-2x20-2x5min^{-}	700	20	5	Without gas

3.5 Coating Characterization

Some of the coatings were characterized with regards to composition, microstructure and thermal behavior.

3.5.1 Chemical Composition and Microstructure

The phase composition of the coatings was determined using the D8 Focus X-ray diffractometer, with Cu Kα radiation. The substrates with coatings were mounted on circular sample holders using glazier's putty.

To identify the different components in the coatings, Fourier Transform Infrared (FTIR) spectroscopy was performed by use of a vacuum FTIR spectrometer (IFS 66 V, Bruker). FTIR was performed on KBr-pellets in the wavelength range from 500 cm^{-1} to 4000 cm^{-1}. As a background sample pure KBr pellets were used. KBr was dried in a vacuum furnace for 24 hours before it was mixed with 0.5 wt% of coating scratched of the substrate. 0.2 g of the mixture was further pressed to disc shaped pellets.

A low vacuum scanning electron microscope (Hitachi S-3400N) was used to study the microstructure and homogeneity of the coatings. Both the surface and cross sections were examined. Two different coating preparation methods were used for cross section examination. For the non-dried green coatings, it was possible to delaminate the coating off the substrate without introducing defects. For the dried coatings it was necessary to scratch off some of the coating at one edge and examine cross sections of the whole sample. For the dried coatings, the samples were coated with gold before examination in SEM.

To compare the chemical composition of different phases of the coatings observed in the SEM, Energy Dispersive X-ray Spectroscopy (EDS) was performed.

3.5.2 Thermal Behavior

The mass loss of the coatings was measured as a function of increasing temperature by TGA on coating scratched off the substrate. TGA was performed on a STA 449C Jupiter from Netzsch. A mass spectrometer was coupled to the equipment to detect gas evolution as a function of temperature. The experiments were conducted in flowing synthetic air with a heating rate of 10 °C per minute up to 1000 °C.

4 Results

4.1 Powder Characterization – Chemical Composition

The diffractograms in Figure 4.1 present XRD results of 8YSZ, 4YSZ, 3YSZ and 1.5YSZ powders made from precursor solutions with molar ratios of 3:97, 6:94, 8:92 and 16:84 of Y to Zr calcined at 1100 °C for 2 hours. It can be seen that the powder was pure and crystalline. In Figure A.1, Figure A.2, Figure A.3 and Figure A.4 in Appendix A the diffractograms of respectively 8YSZ, 4YSZ, 3YSZ and 1.5YSZ powders are shown individually. Diffraction lines associated with the different phases are included in the figures. For 8YSZ powder, a cubic phase was stabilized. For 4YSZ, 3YSZ and 1.5YSZ powders, both tetragonal and monoclinic phases were present. As shown in Figure 4.1, the amount of tetragonal phase decreased and the amount of monoclinic phase increased when the amount of Y_2O_3 was decreased.

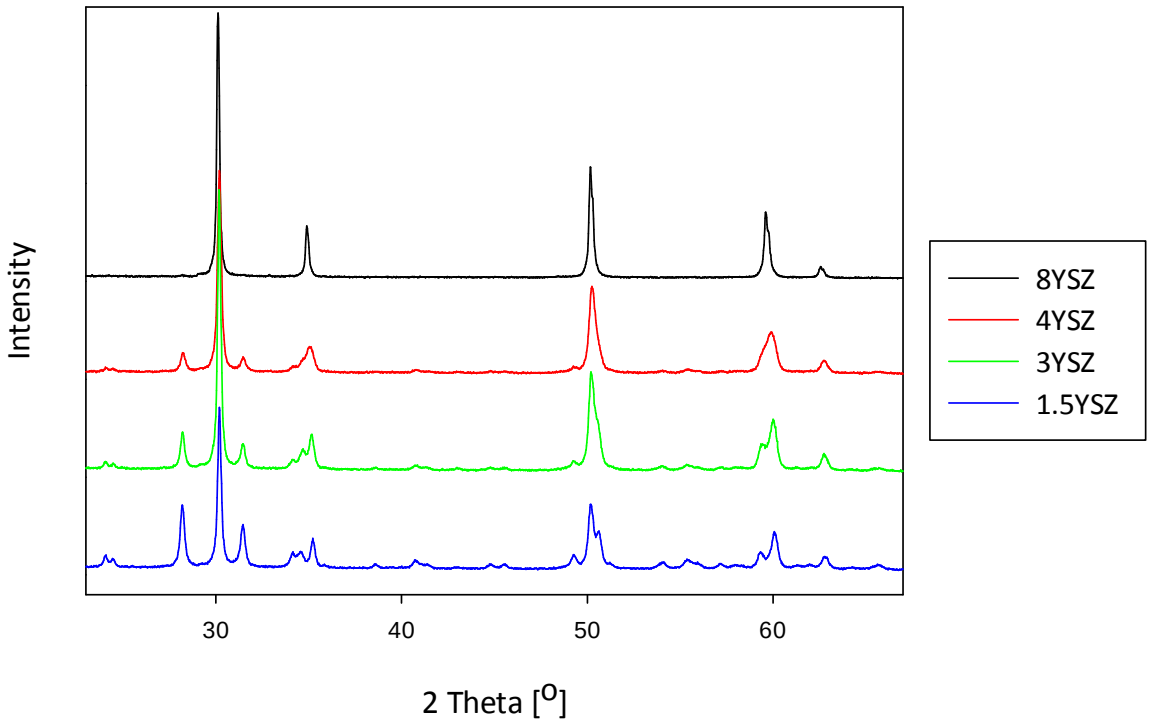

Figure 4.1: Diffractograms of 8YSZ, 4YSZ, 3YSZ and 1.5YSZ powders calcined at 1100 °C for 2 hours.

4.2 Spray Pyrolysis

4.2.1 Set-Point Temperature

Figure 4.2 presents thermogravimetric analysis of 1.5YSZ, 3YSZ, 4YSZ and 8YSZ powders. Included in the figure is the first derivative of the mass as a function of temperature for 8YSZ. The first mass loss starts at around 100 °C and is attributed to the evaporation of the crystal water in the structure. At a temperature of approximately 210 °C, a second mass loss starts attributed to the decomposition of nitrates. It is preferable to do the spray pyrolysis at a temperature high enough to evaporate most of the water during transport to the substrate before decomposition. However, because the deposition of an ionic salt liquid is required, complete decomposition of the nitrates should be avoided. Based on the first derivative in Figure 4.2, set-point temperatures in the range 650 to 800 °C were used to prepare the coatings. The different set-point temperatures are included in the graph as vertical lines. Set-point temperatures of 650 °C, 700 °C, 750 °C and 800 °C respectively corresponds to substrate temperatures of 165 °C, 192 °C, 216 °C and 240 °C during spray pyrolysis (see Table 3.2).

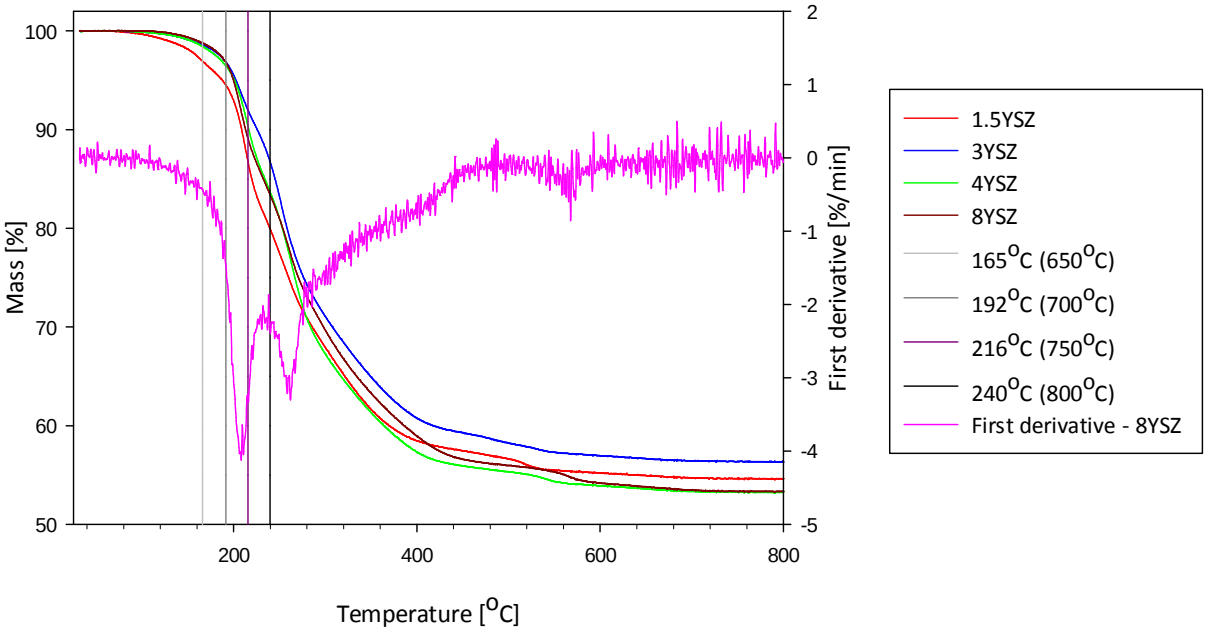

Figure 4.2: TGA of 1.5YSZ, 3YSZ, 4YSZ and 8YSZ powders showing mass as a function of temperature. The first derivative of the mass as a function of temperature for 8YSZ is also included in the figure.

4.2.2 Preliminary Tests

Pictures of coatings 1-5 prepared with spray pyrolysis parameters described in Table 3.4 are shown in Figure 4.3. The pictures were taken immediately after spray pyrolysis.

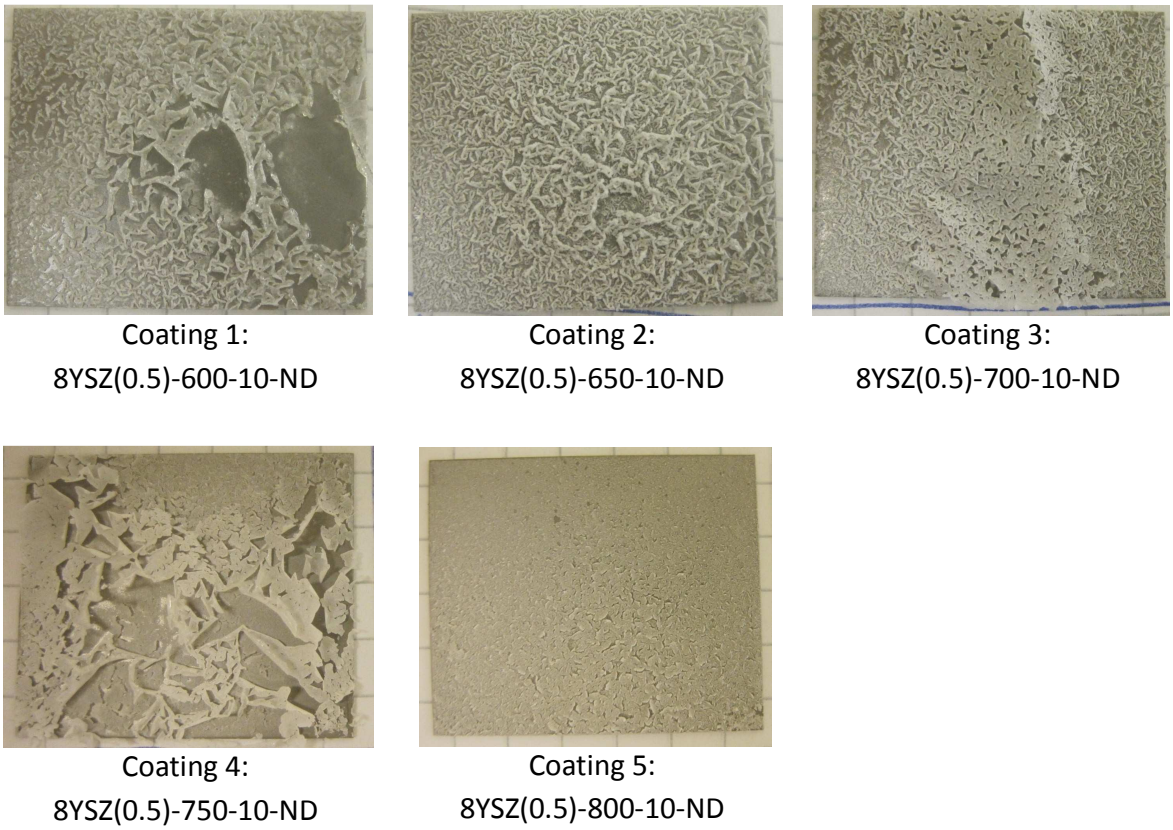

Coating 1: 8YSZ(0.5)-600-10-ND

Coating 2: 8YSZ(0.5)-650-10-ND

Coating 3: 8YSZ(0.5)-700-10-ND

Coating 4: 8YSZ(0.5)-750-10-ND

Coating 5: 8YSZ(0.5)-800-10-ND

Figure 4.3: Pictures of coatings 1-5 prepared from the 0.5 M precursor solution of 8YSZ. The pictures were taken directly after spray pyrolysis.

Pictures of coatings 6-15 prepared with spray pyrolysis parameters as described in Table 3.5 are shown in Figure 4.4. The pictures were taken immediately after spray pyrolysis.

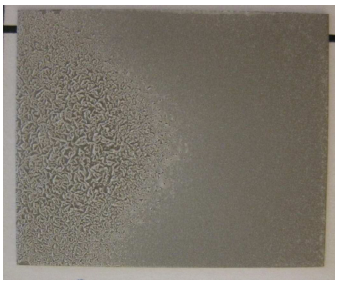

Coating 6:
8YSZ(0.25)-650-10-ND

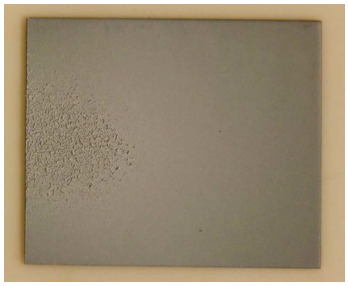

Coating 7:
8YSZ(0.25)-675-10-ND

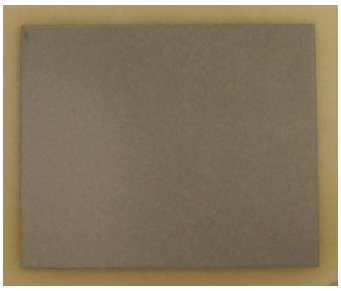

Coating 8:
8YSZ(0.25)-700-10-ND

Coating 9:
8YSZ(0.25)-700-10-5min-

Coating 10:
8YSZ(0.25)-700-10-15min-

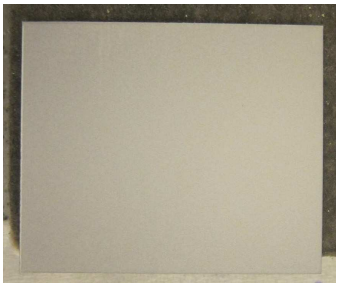

Coating 11:
8YSZ(0.25)-700-20-ND

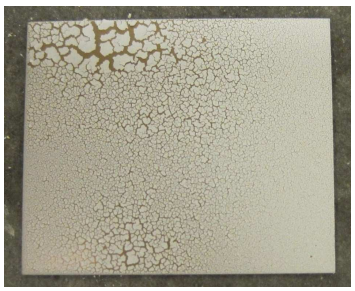

Coating 12:
8YSZ(0.25)-700-20-15min-

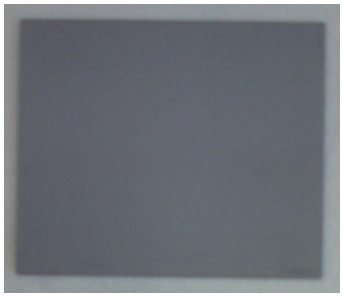

Coating 13:
8YSZ(0.25)-700-5-ND

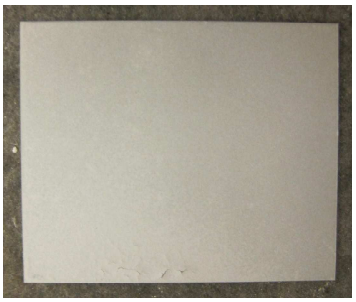

Coating 14:
8YSZ(0.25)-725-10-ND

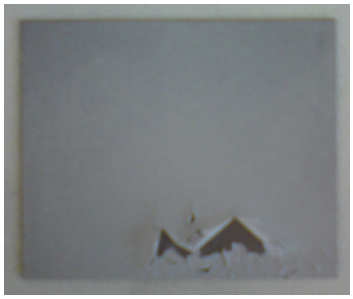

Coating 15:
8YSZ(0.25)-750-10-ND

Figure 4.4: Pictures of coatings 6-15 prepared from the 0.25 M precursor solution of 8YSZ. The pictures were taken directly after spray pyrolysis.

Pictures of coatings 16-21 prepared with the spray pyrolysis parameters described in Table 3.6 are shown in Figure 4.5. The pictures were taken immediately after spray pyrolysis.

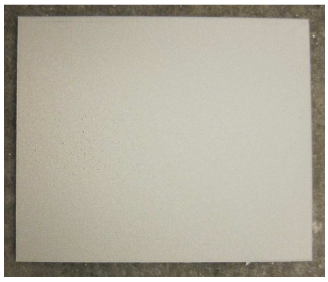

Coating 16:
8YSZ(0.125)-650-20-ND

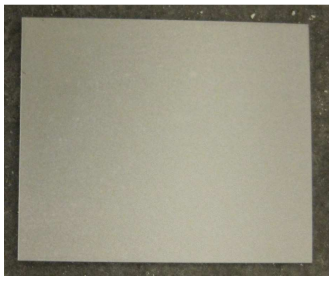

Coating 17:
8YSZ(0.125)-700-20-ND

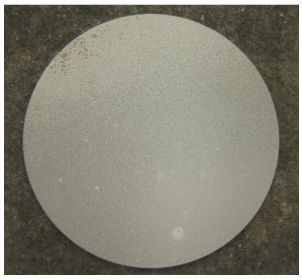

Coating 18:
8YSZ(0.125)-700-20-5min^{+}

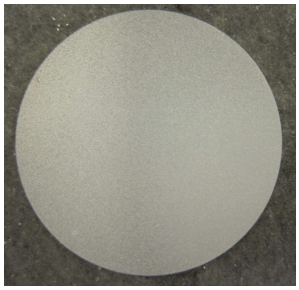

Coating 19:
8YSZ(0.125)-700-20-5min^{-}

Coating 20:
8YSZ(0.125)-700-20-15min^{-}

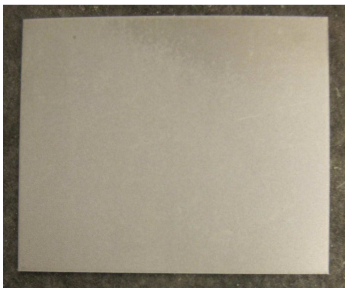

Coating 21:
8YSZ(0.125)-750-20-ND

Figure 4.5: Pictures of coatings 16-21 prepared from the 0.125 M precursor solution of 8YSZ. The pictures were taken directly after spray pyrolysis.

All coatings prepared with 10 ml of the 0.5 M precursor solution were cracked and discontinuous with poor adhesion to the substrate. By decreasing the concentration of the precursor solution to 0.25 M or 0.125 M, improved coatings were deposited depending on the spray pyrolysis parameters.

4.2.3 Deposition Temperature

Figure 4.6 and Figure 4.7 show SEM micrographs of the microstructure of coatings prepared from respectively the 0.25 M and the 0.125 M precursor solution with a volume of 10 ml and 20 ml sprayed at different set-point temperatures. The coatings were sprayed without drying on the heating plate and micrographs of the surface were taken immediately after spray pyrolysis. The cross section micrographs were taken some days after spray pyrolysis when the coatings had delaminated from the substrate (described in Section 4.2.4).

a) Coating 6: 8YSZ(0.25)-650-10-ND

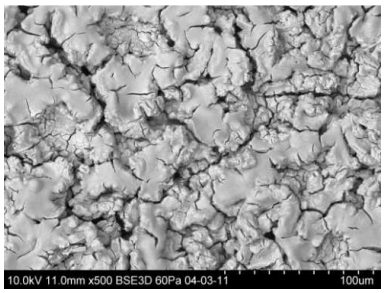

b) Coating 7: 8YSZ(0.25)-675-10-ND

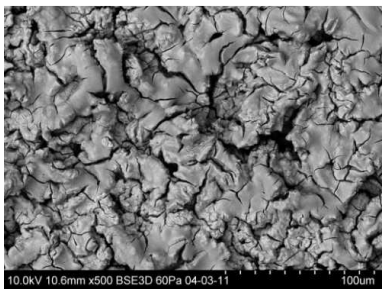

c) Coating 8: 8YSZ(0.25)-700-10-ND

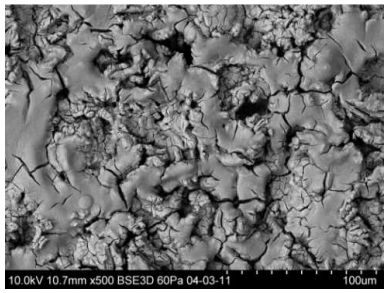

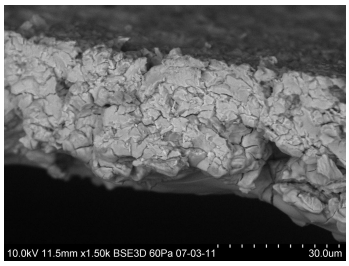

Thickness = 28 µm

d) Coating 14: 8YSZ(0.25)-725-10-ND

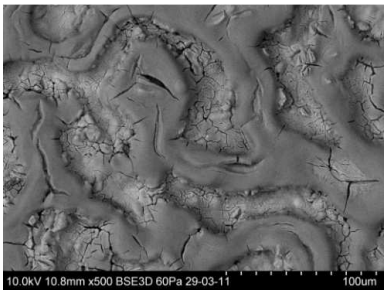

e) Coating 15: 8YSZ(0.25)-750-10-ND

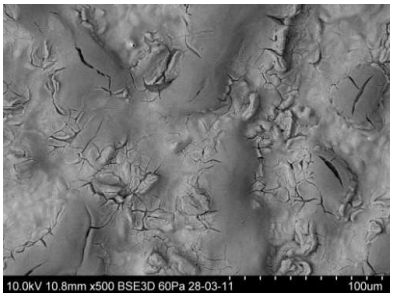

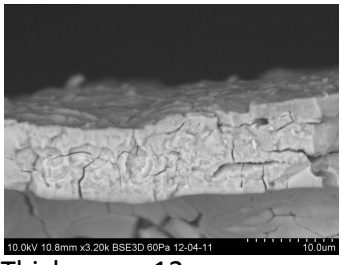

Thickness = 12 µm

Figure 4.6: SEM micrographs of coatings prepared from the 0.25 M precursor solution. The coatings are sprayed at varying set-point temperatures (increasing set-point temperature from **a**-**e**) and without drying on the heating plate. For coating 8 (**c**) and 15 (**e**) cross section images are included.

a) Coating 16: 8YSZ(0.125)-650-20-ND

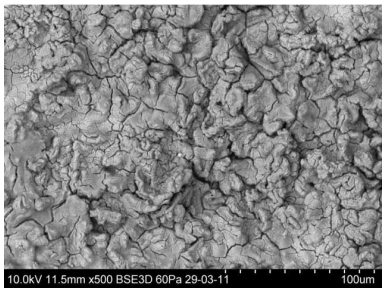

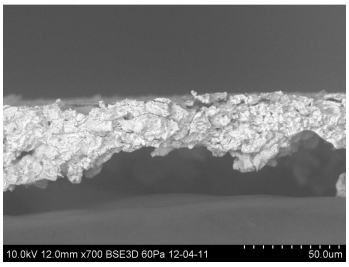

Thickness = 32 µm

b) Coating 17: 8YSZ(0.125)-700-20-ND

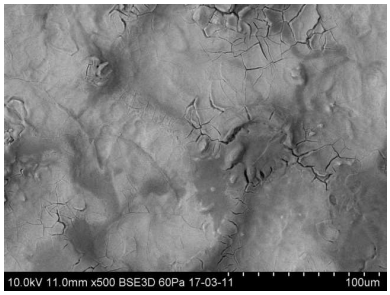

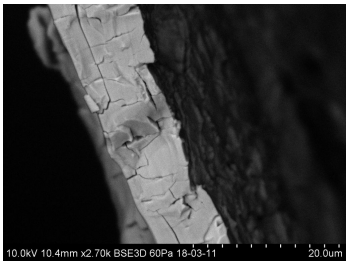

Thickness = 12 µm

c) Coating 21: 8YSZ(0.125)-750-20-ND

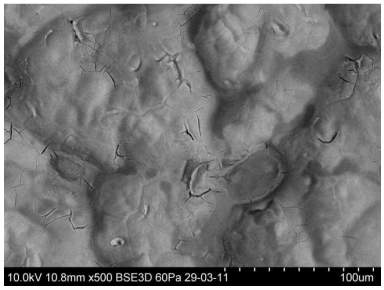

Figure 4.7: SEM micrographs of coatings prepared from the 0.125 M precursor solution. The coatings are sprayed at varying set-point temperatures (increasing set-point temperature from **a-c**) and without any drying on the heating plate. For coating 16 (**a**) and 17 (**b**) cross section micrographs taken one day after spraying are included.

As observed in Figure 4.6 and Figure 4.7, both the microstructure and the thickness of the coatings changed with temperature. The density of cracks was observed to decrease with increasing substrate temperature. For the coatings in Figure 4.6 prepared from the high concentration precursor (0.25 M), a substantial change in microstructure took place between set-point temperatures of 700 and 725 °C. For the coatings in Figure 4.7 prepared from the low concentration precursor (0.125 M), the microstructure changed in the same way between 650 and 700 °C. The cross section micrographs in Figure 4.6 and Figure 4.7 show that the coating thickness decreased with increasing substrate temperature. Coatings 8YSZ(0.25)-700-10-ND and 8YSZ(0.125)-650-20-ND were in the same thickness range while coatings 8YSZ(0.25)-750-10-ND and 8YSZ(0.125)-750-20-ND were about half the thickness.

The structure of coatings 6, 7, 8 (Figure 4.6 a, b and c) and 16 (Figure 4.7 a) will be referred to as the “low temperature structure” and the structure of coating 14, 15 (Figure 4.6d and e), 17 and 21 (Figure 4.7b and c) will be referred to as the “high temperature structure” throughout the rest of the report. The coatings with the “low temperature structure” were covered with cracks, while the “high temperature structure” was approximately crack-free.

Coatings 8YSZ(0.25)-700-10-ND, 8YSZ(0.125)-650-20-ND, 8YSZ(0.125)-700-20-ND and 8YSZ(0.125)-750-ND (shown in Figure 4.6 c and Figure 4.7 a, b and c respectively) sprayed without drying were further characterized by TG and FTIR.

Figure 4.8 presents thermogravimetric analysis of coatings 8YSZ(0.125)-650-20-ND, 8YSZ(0.125)-700-20-ND, 8YSZ(0.125)-750-20-ND and 8YSZ(0.25)-700-10-ND sprayed without drying on the heating plate.

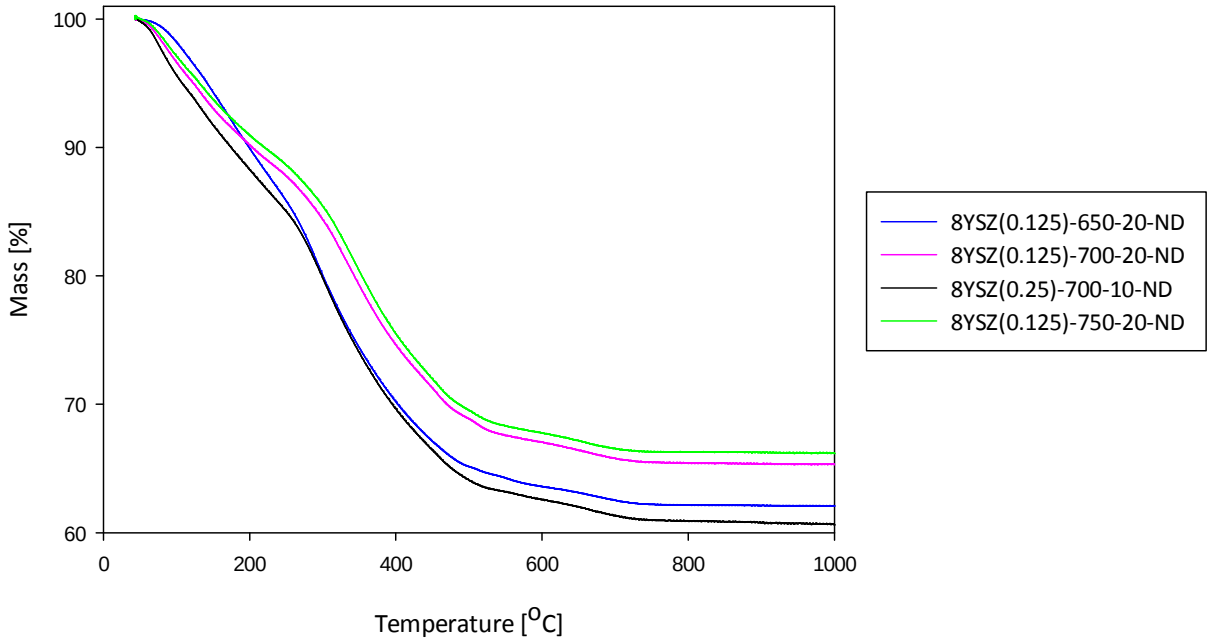

Figure 4.8: TGA of coatings 8YSZ(0.125)-650-20-ND, 8YSZ(0.125)-700-20-ND, 8YSZ(0.125)-750-20-ND and 8YSZ(0.25)-700-10-ND sprayed without drying on the heating plate.

As Figure 4.8 shows, the coatings lost masses in three steps. The first loss starting at approximately 100 °C is attributed to the crystal water in the structure and water absorbed after spray pyrolysis. The second loss starting at approximately 210 °C is attributed to the nitrate decomposition. The smaller third mass loss starts at approximately 600 °C and is believed to be due to the decomposition of carbonates. The biggest mass losses are observed for coating 8YSZ(0.125)-650-20-ND and coating 8YSZ(0.125)-700-20-ND, the two coatings with the "low temperature structure".

The evolution of water vapor was measured as a function of temperature by mass spectrometer during TGA and the results are presented in Figure 4.9.

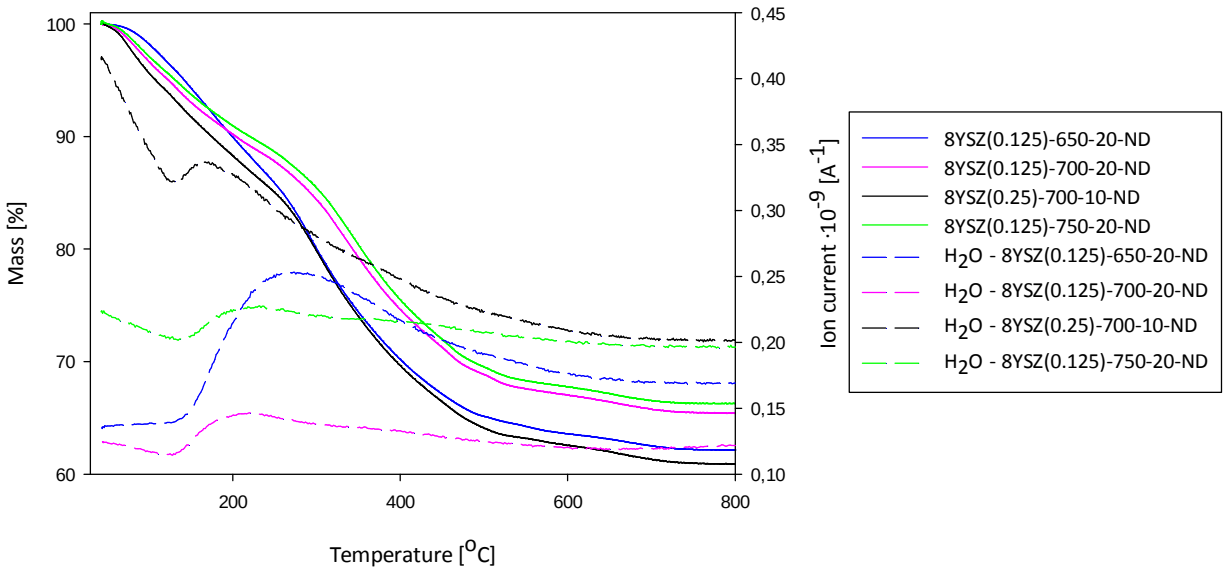

Figure 4.9: Water vapor evolution as a function of temperature during TGA.

The evolution of nitrates (NO and NO_2 gas) was also measured as a function of temperature during TGA and the results are presented in Figure 4.10.

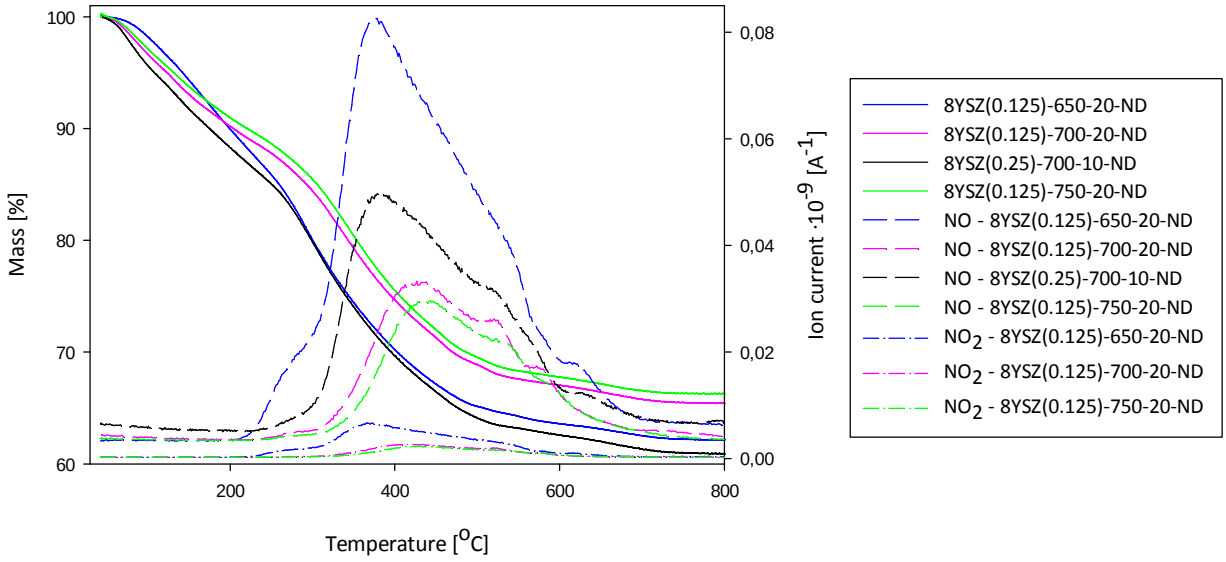

Figure 4.10: NO and NO_2 gas evolution as a function of temperature during TGA.

The mass spectrometry measurements agree well with the TGA results. Bigger amount of evolved gas, were detected for coatings 8YSZ(0.125)-650-20-ND and 8YSZ(0.25)-700-10-ND with the "low temperature structure" compared to the "high temperature coatings".

Figure 4.11 presents FTIR spectra of coatings 8YSZ(0.125)-650-20-ND, 8YSZ(0.125)-700-20-ND, 8YSZ(0.125)-750-20-ND and 8YSZ(0.25)-700-10-ND.

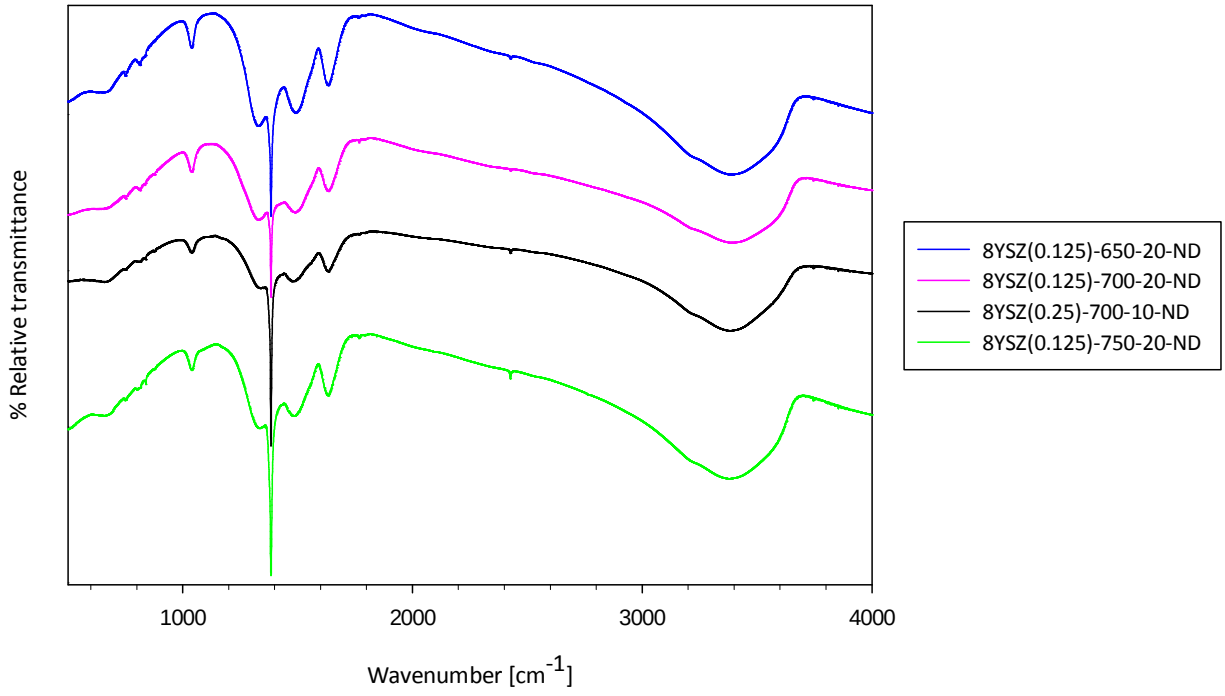

Figure 4.11: FTIR spectra of coatings 8YSZ(0.125)-650-20-ND, 8YSZ(0.125)-700-20-ND, 8YSZ(0.125)-750-20-ND and 8YSZ(0.25)-700-10-ND.

A closer look at the FTIR results for coating 8YSZ(0.125)-650-20-ND is shown in Figure 4.12. The individual FTIR spectra for coatings 8YSZ(0.125)-700-20-ND, 8YSZ(0.125)-750-20-ND and 8YSZ(0.25)-700-10-ND are shown in Figure B.1, Figure B.2 and Figure B.3 in Appendix B respectively. The same characteristic bands are observed for all four coatings with approximately the same intensities. The broad band in the region of 3000-3600 cm^{-1} corresponds to the O-H stretching vibrations [31]. The band at 1635 cm^{-1} is assigned to the bending mode of lattice-coordinated water [32] and the bands in the region 1250-1600 cm^{-1} are attributed to the v_3 vibrational mode of NO_3^- [31]. The splitting of this band is caused by the decrease of symmetry of the NO_3^- molecule when it is coordinated with Y^{3+} and Zr^{4+} [8]. Due to the sharpness of the band at 1384 cm^{-1} it is believed to be attributed to surface absorbed NO_2 [33]. The band at 1039 cm^{-1} corresponds to the v_1 vibrational mode of NO_3^- [31].

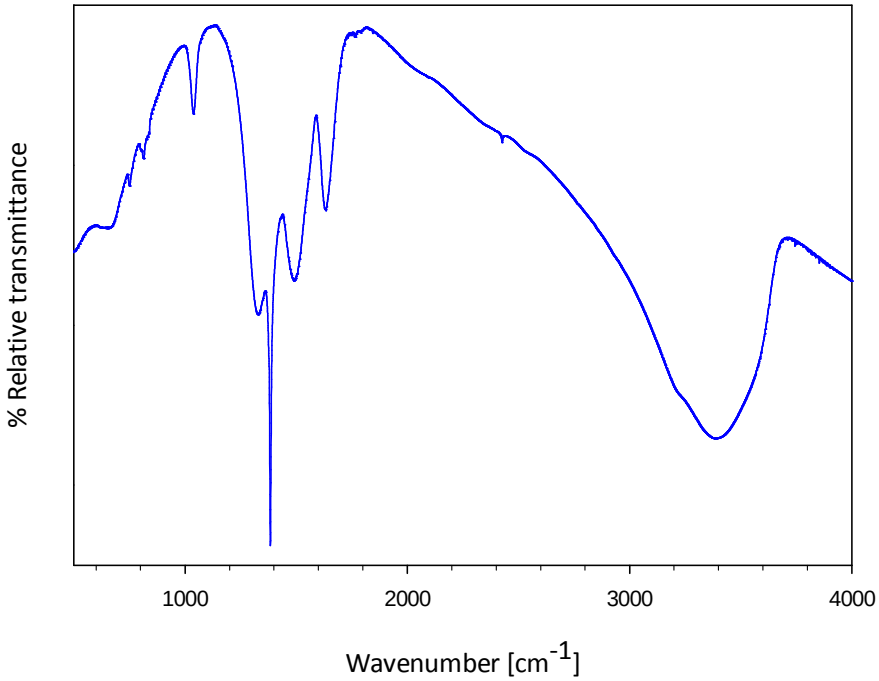

Figure 4.12: FTIR spectrum of coating 8YSZ(0.125)-650-20-ND. Several bands can be distinguished.

4.2.4 Microstructure

Representing respectively the "low temperature structure" and the "high temperature structure" coating 8YSZ(0.25)-700-10-ND and coating 8YSZ(0.125)-700-20-ND were examined further.

Coatings sprayed without drying delaminated from the substrate one day after spraying, making it possible to examine easily the microstructure from above and from beneath as illustrated in Figure 4.13. Microstructure micrographs taken from above and from beneath are shown for coating 8YSZ(0.25)-700-25-10-ND and coating 8YSZ(0.125)-700-25-20-ND in Figure 4.14. From above, the coating surface is observed to be rougher than the interface surface between the substrate and the coating. However, the microstructure of the two surfaces looks similar.

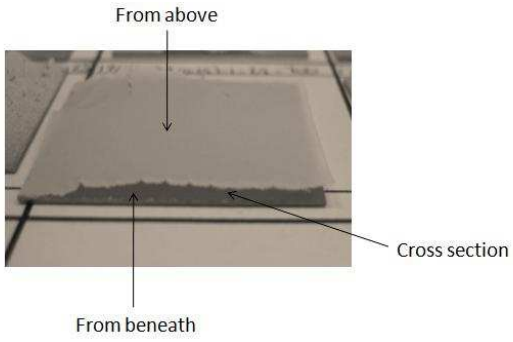

Figure 4.13: Coatings sprayed without drying delaminated from the substrate one day after spraying. Microstructure examination was performed from above the coating and from beneath.

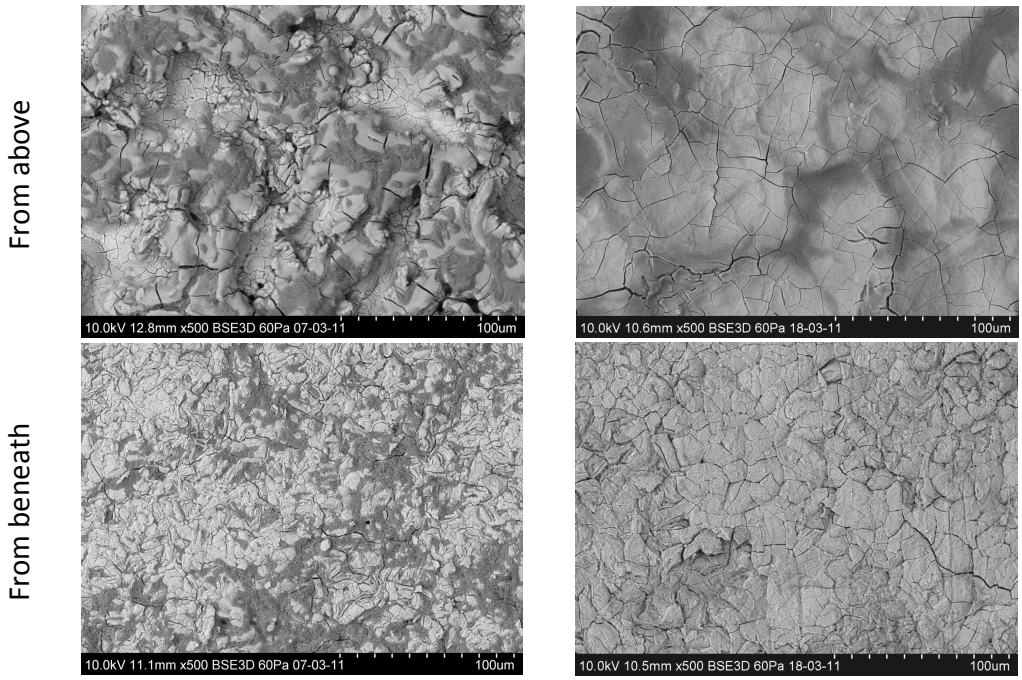

a) 8YSZ(0.25)-700-10-ND b) 8YSZ(0.125)-700-20-ND

Figure 4.14: Micrographs of delaminated coatings of 8YSZ(0.25)-700-10 (**a**) and 8YSZ(0.125)-700-20 (**b**) after spray pyrolysis deposition without drying.

As shown in Figure 4.14a two different phases were observed in the coating one day after spray pyrolysis. The same phenomenon was not observed for the same coating in Figure 4.6c when the micrograph was taken immediately after spray pyrolysis, indicating an ageing issue. Figure 4.15 and Table 4.1 present EDS results for the two different phases. It can be seen that the bright phase was rich in zirconium while the dark phase was rich in yttrium.

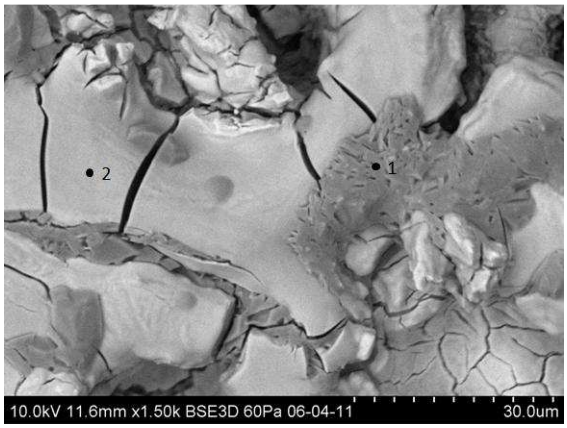

Figure 4.15: Two different phases were observed in the aged coating 8YSZ(0.25)-700-10-ND after spray pyrolysis. EDS measurements were done on the dark phase (1) and the bright phase (2).

Table 4.1: EDS results for coating 8YSZ(0.25)-700-10-ND.

Measurement	N [wt%]	O [wt%]	Y [wt%]	Zr [wt%]	Total
1	8.24	41.24	35.67	14.85	100.00
2	6.13	35.96	14.70	43.21	100.00

4.2.5 Heat Treatment

The diffractograms in Figure 4.16 show XRD results for coatings 8YSZ(0.25)-700-10-ND and 8YSZ(0.125)-700-20-ND sprayed without drying on the heating plate. The broad peak at approximately 30° in the diffractograms indicates that the coatings had an amorphous structure with a low degree of crystallinity after deposition.

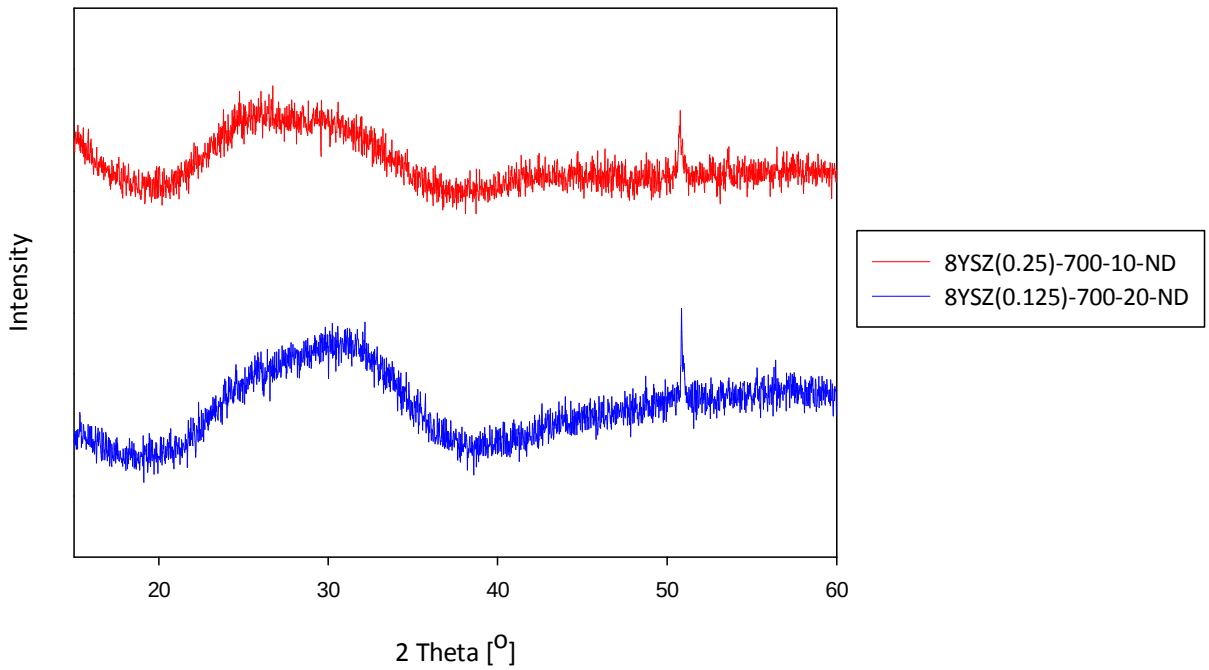

Figure 4.16: Diffractograms of coatings 8YSZ(0.25)-700-10-ND and 8YSZ(0.125)-700-20-ND after spray pyrolysis.

Micrographs of coatings 8YSZ(0.25)-700-10-15min^{-} and 8YSZ(0.125)-700-20-15min^{-} dried for 15 minutes without gas supply and coatings 8YSZ(0.25)-700-10-5min^{+} and 8YSZ(0.125)-700-20-5min^{-} dried for 5 minutes with and without gas respectively are shown in Figure 4.17. When the set-point temperature was fixed at 700 °C, sprayed coatings dried on the heating plate with or without gas supply were exposed to maximum temperatures of respectively 190 or 440 °C during drying.

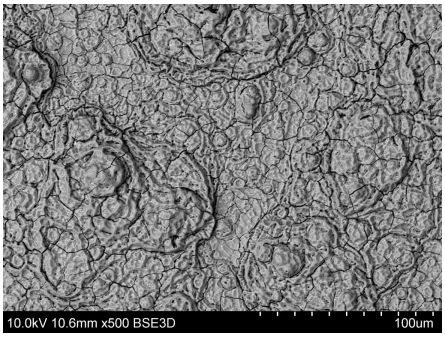

a) 8YSZ(0.125)-700-20-5min^{+}

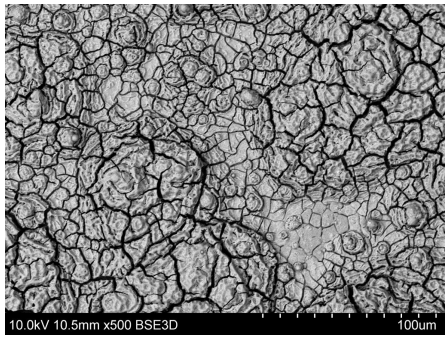

b) 8YSZ(0.125)-700-20-5min^{-}

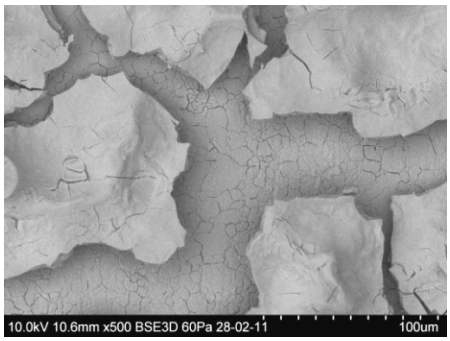

c) 8YSZ(0.125)-700-20-15min^{-}

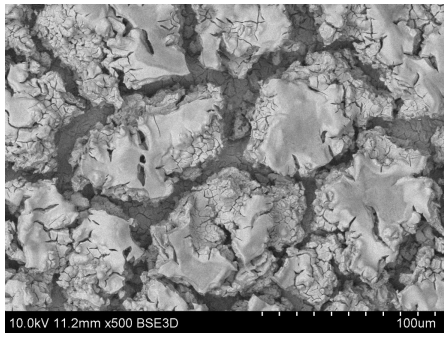

d) 8YSZ(0.25)-700-10-15min^{-}

Figure 4.17: Microstructure examination of coatings 8YSZ(0.125)-700-20-5min^{+} (**a**), 8YSZ(0.125)-700-20-5min^{-} (**b**), 8YSZ(0.125)-700-20-15min^{-} (**c**) and 8YSZ(0.25)-700-10-15min^{-} (**d**).

Comparing the structure of coatings 8YSZ(0.25)-700-10-ND in Figure 4.6c and 8YSZ(0.25)-700-10-15min^{-} in Figure 4.17d, the density and size of the cracks are observed to increase during heat treatment. Comparing the structure of coating 8YSZ(0.125)-700-20-ND in Figure 4.7b to the structures in Figure 4.17a, b and c, it can be seen that cracks are introduced into the coating during heat treatment. Coating 8YSZ(0.125)-700-20-5min^{+} (Figure 4.17a), dried with gas, is less cracked than coating 8YSZ(0.125)-700-20-5min^{-} (Figure 4.17b), dried without gas. Comparing the structure of coatings 8YSZ(0.125)-700-20-5min^{-} and 8YSZ(0.125)-700-20-15min^{-}, the crack size is observed to increase with increasing drying time.

Pictures of coatings 8YSZ(0.25)-700-10-SH and 8YSZ(0.125)-700-20-SH heat treated to 600 °C for 2 hours with heating and cooling rates of 5 °C/h are shown in Figure 4.18a and b respectively. Coating 8YSZ(0.25)-700-10-SH still showed good adhesion to the substrate after heat treatment while coating 8YSZ(0.125)-700-20-SH delaminated from the substrate in some areas. Micrographs of the surface microstructure of coating 8YSZ(0.25)-700-10-SH are shown in Figure 4.19. As observed in Figure 4.19, the density and size of the cracks had increased for coating 8YSZ(0.25)-700-10-SH compared to coating 8YSZ(0.25)-700-10-ND in Figure 4.6c. The crack size were observed to be larger for coating 8YSZ(0.25)-700-10-SH compared to 8YSZ(0.25)-700-10-15min^{-}.

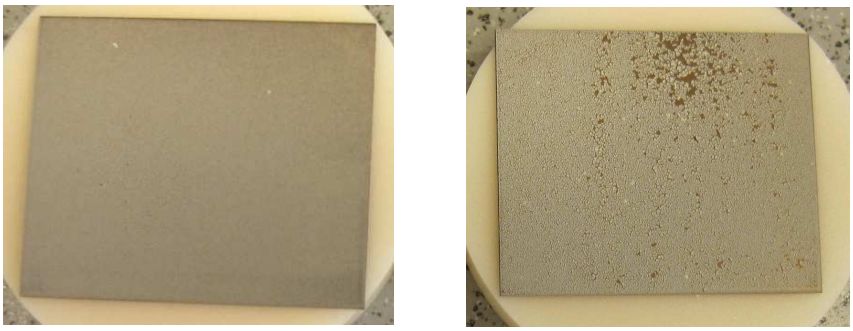

a) 8YSZ(0.25)-700-10-SH b) 8YSZ(0.125)-700-20-SH

Figure 4.18: Pictures taken of coatings 8YSZ(0.25)-700-10-SH (**a**) and 8YSZ(0.125)-700-20-SH (**b**) after slow heating to 600 °C for 2 hours with heating and cooling rates of 5 °C/h.

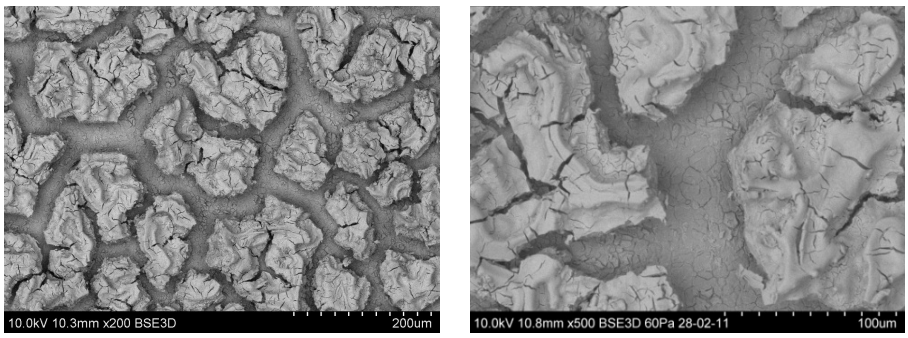

Figure 4.19: Microstructure examination of coating 8YSZ(0.25)-700-10 after slow heating to 600 °C for 2 hours with heating and cooling rates of 5 °C/h. Micrographs are taken with two different magnifications.

4.2.6 Multi-Layered Coatings

Pictures of the two-layered coatings 24 and 25 sprayed with the parameters described in Table 3.8 are shown in Figure 4.20a and b respectively. Coating 24 dried for 5 minutes with gas (8YSZ(0.125)-700-2x20-2x5min^{+}) was exposed to a substrate temperature of 192 °C during drying and coating 25 dried for 5 minutes without gas (8YSZ(0.125)-700-2x20-2x5min^{-}) was exposed to a substrate temperature of 440 °C during drying.

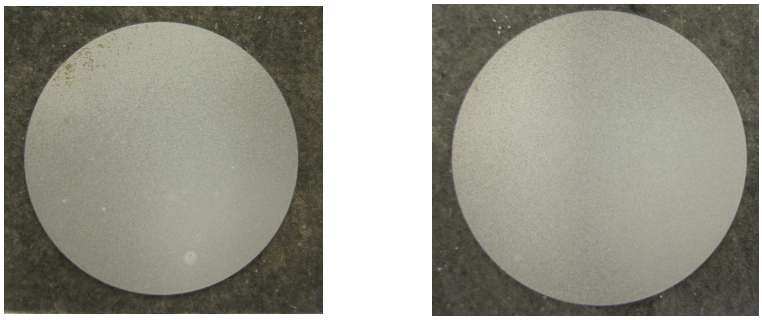

a) Coating 24: 8YSZ(0.125)-700-2x20-2x5min^{+} b) Coating 25: 8YSZ(0.125)-700-2x20-2x5min^{-}

Figure 4.20: Pictures of coatings 8YSZ(0.125)-700-2x20-2x5min^{+} (**a**) and 8YSZ(0.125)-700-2x20-2x5min^{-} (**b**) sprayed at 700 °C taken immediately after spray pyrolysis.

It can be seen that the coatings were still continuous and had good adhesion to the substrate after the second layer was deposited. Micrographs of the surface microstructure of coatings 8YSZ(0.125)-700-2x20-2x5min^{+} and 8YSZ(0.125)-700-2x20-2x5min^{-} are shown in Figure 4.21b and d respectively. As a comparison microstructure micrographs of coating 18 and 19 sprayed with only one layer and 5 minutes drying with and without gas are included in Figure 4.21a and c. After deposition of the second layer the surface seemed to be more flat and homogenous compared to the one-layered coatings. The density and size of the cracks were observed to be higher for coatings dried without gas (Figure 4.21a and b) compared to the coatings dried with gas (Figure 4.21c and d).

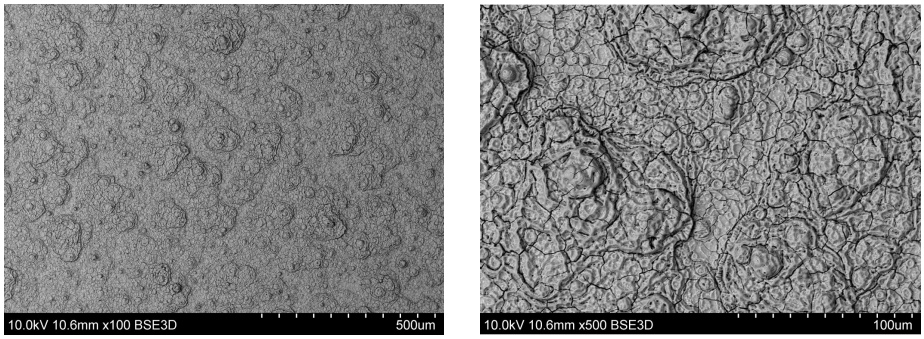

a) 8YSZ(0.125)-700-20-5min^{+}

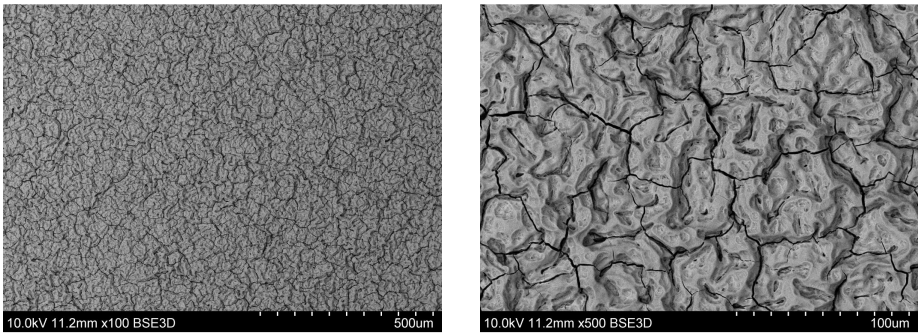

b) 8YSZ(0.125)-700-2x20-2x5min^{+}

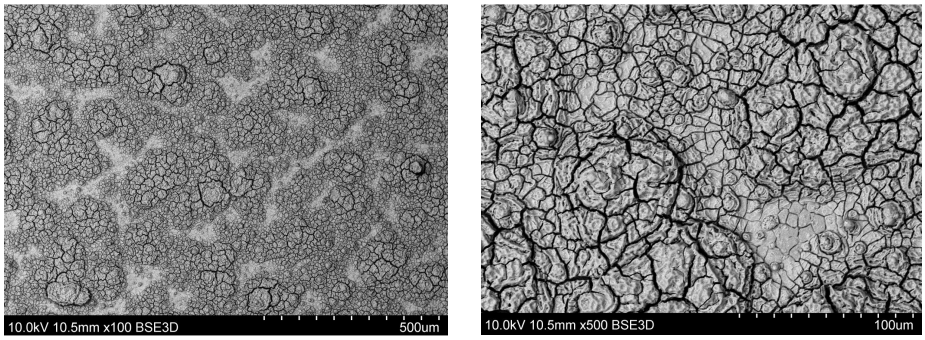

c) 8YSZ(0.125)-700-20-5min^{-}

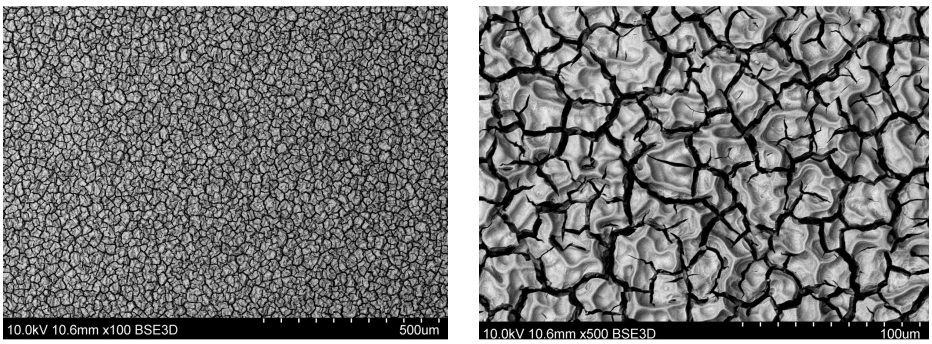

d) 8YSZ(0.125)-700-2x20-2x5min^{-}

Figure 4.21: Micrographs of the surface microstructure of coating 8YSZ(0.125)-700-20-5min^{+} (**a**), 8YSZ(0.125)-700-2x20-2x5min^{+} (**b**), 8YSZ(0.125)-700-20-5min^{-} (**c**) and 8YSZ(0.125)-700-2x20-2x5min^{-} (**d**).

Figure 4.22 shows the cross section of coating 8YSZ(0.125)-700-2x20-2x5min^{+}. As observed in the figure it is not possible to distinguish the two layers individually. From cross section examination in SEM the thickness of coating 8YSZ(0.125)-700-2x20-2x5min^{+} and 8YSZ(0.125)-700-2x20-2x5min^{-} was estimated to be around 26 and 25 µm respectively, which is approximately twice the coating thickness of the one-layered coating 8YSZ(0.125)-700-20-ND sprayed without drying on the heating plate shown in Figure 4.7b.

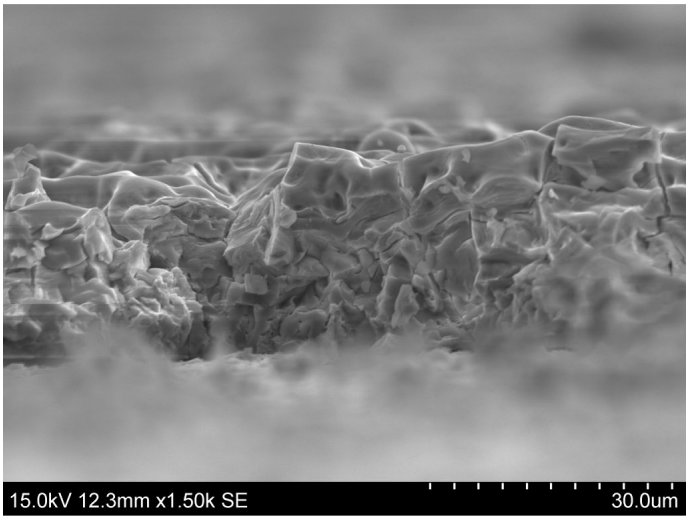

Figure 4.22: Cross section micrograph of coating 8YSZ(0.125)-700-2x20-2x5min^{+}.

5 Discussion

5.1 Powder Characterization – Chemical Composition

The XRD results showed that the powder was pure and crystalline with the correct stoichiometry.

As described in Section 2.5.2 the preferred high temperature tetragonal and cubic phases of zirconia can be stabilized down to room temperature by aliovalent substitution of lower valent oxides such as Y_2O_3. For the 8YSZ powder the amount of Y_2O_3 was shown to be high enough for the cubic phase to be stabilized at room temperature. For the 4YSZ powder the tetragonal phase was the dominating phase and just small amounts of the monoclinic phase were present. When decreasing the amount of Y_2O_3, the amount of tetragonal phase was decreased and the amount of monoclinic phase was increased as shown in Figure 4.1 for the 3YSZ and 1.5YSZ powders. This trend is in good agreement with the zirconia rich part of the phase diagram shown in Figure 2.5.

5.2 Spray Pyrolysis

5.2.1 Set-Point Temperature

With thermogravimetric analysis it was shown to be possible to estimate a temperature range for the set-point temperature to be used during spray pyrolysis. To avoid deposition of droplets on the substrate it is preferable to spray the substrate at a temperature high enough to evaporate most of the water during transport to the substrate. However, because the deposition of an ionic salt liquid is required, complete decomposition of nitrates should be avoided. In addition, if the decomposition of nitrates completes during transport to the substrate unwanted oxide particles will be deposited. Therefore, as described in Section 2.6.2, for a given precursor solution there is a specific temperature window where it is possible to get crack-free green coatings.

As shown in Figure 4.2, the first mass loss starts at approximately 100 °C and is attributed to the evaporation of the crystal water in the structure. At a temperature at approximately 210 °C, a second mass loss starts attributed to the decomposition of nitrates. Therefore, to find the temperature window for crack free green coatings of 8YSZ, set-point temperatures in the range 650-800 °C were used to prepare coatings.

It is worth noting the fact that during TGA the mass was measured as a function of temperature for a specific heating rate. Changing the heating rate will delay or enhance the mass losses according to temperature. A heating rate of 10 °C/min was used during the experiments. Even though the temperature gradient experienced by the droplets during transport was also relatively large, the measurements were not totally comparable to the spray pyrolysis process. As a consequence it was important to spray coatings in a wider temperature range than the

temperature range estimated by TGA to find the interval for the deposition of crack-free green coatings.

5.2.2 Preliminary Tests

As shown in Figure 4.3, all coatings sprayed from 10 ml of the 0.5 M precursor solution were cracked and discontinuous with poor adhesion to the substrate. Due to the fact that for the same volume, a decrease in concentration of the precursor solution led to an improvement of the coatings, it is believed that coatings 1-5 cracked because of a too large volume sprayed. A precursor solution with a high concentration contains a large amount of reactants per volume to evaporate during transport and decompose after deposition. Therefore, a combination of high concentration and volume generates stresses in the deposited film which can result in cracking and delamination.

During spray pyrolysis of coatings 1-5, it was observed that the coatings were continuous during spraying until a critical volume was deposited and the cracking started. These observations are in agreement with the statement above indicating a too large sprayed volume.

These observations show that for a given precursor solution concentration, there is a maximum film thickness achievable before spallation of the coating due to built-up stresses which exceed the fracture toughness of the material. To compensate for a high concentration, the volume sprayed must be lowered. However, decreasing the deposited volume gives a decreased coating thickness. To compensate for the smaller thickness of the film, there is a possibility of spraying multi-layered coatings (discussed in more detail in Section 5.2.6).

5.2.3 Deposition Temperature

As discussed in Section 2.6.2, the substrate temperature has been proposed as the most important adjustable parameter during spray pyrolysis in the literature [28]. Figure 5.1 shows a comparison of the microstructure of coatings 8YSZ(0.25)-700-10-ND and 8YSZ(0.125)-700-20-ND representing respectively the “low temperature structure” and the “high temperature structure”. The “low temperature structure” (Figure 5.1a) was an inhomogeneous structure with a high density of cracks. The “high temperature structure” (Figure 5.1b) was more homogenous with less cracks. From the micrographs of the cross sections, it is shown that the “high temperature structure” wass thinner and denser than the “low temperature structure”.

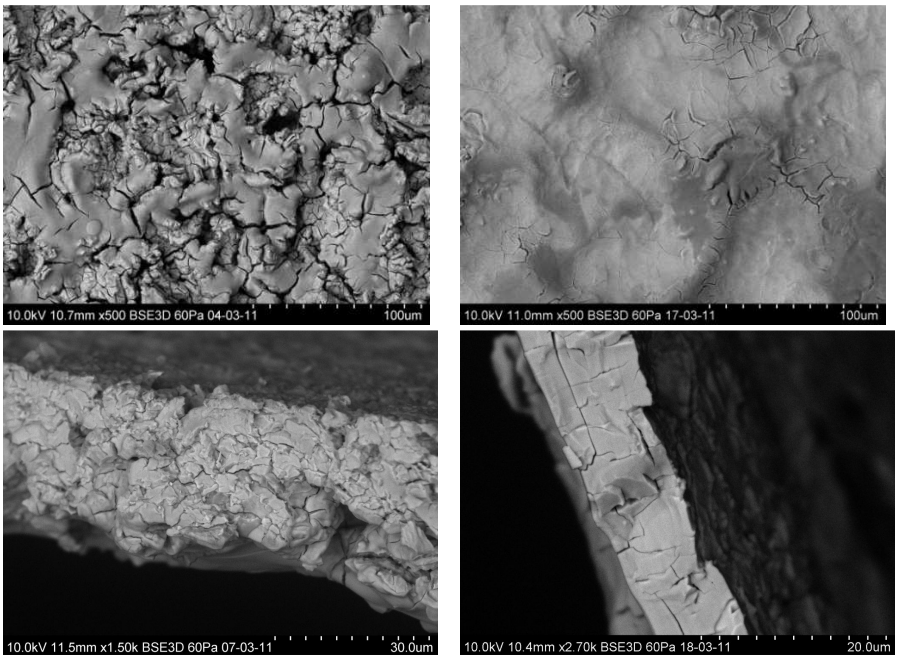

a) 8YSZ(0.25)-700-10-ND b) 8YSZ(0.125)-700-20-ND

Figure 5.1: Micrographs of coatings 8YSZ(0.25)-700-10-ND (**a**) and 8YSZ(0.125)-700-20-ND (**b**) sprayed at 700 °C representing respectively the "low temperature structure" and the "high temperature structure".

The reason for the structure changes can be related to Figure 2.9 illustrating the deposition mechanisms of thick films made by spray pyrolysis. For the "low temperature structure", the temperature is believed to be below the minimum deposition temperature to achieve crack-free green coatings. Droplets are deposited on the substrate resulting in a large amount of solvent still present in the film. The large amount of solvent to evaporate in addition to the salts to decompose induces stress in the deposited film which results in a cracked low density structure. Even though there are a few cracks in the "high temperature coatings", the temperature is believed to be in the temperature interval for crack-free green coating deposition where the solvent evaporates during droplet transport and ionic salt precipitates hits the substrate which results in a crack-free and dense structure.

For the coatings prepared from the 0.25 and 0.125 M precursor solutions, the most distinct changes in microstructure happened between set-point temperatures of 700-725 °C and 650-700 °C respectively. Compared to the coatings prepared from the 0.125 M precursor solution, the microstructure changes occurred at a higher temperature for the coatings prepared from the 0.25 M precursor solution. For the coatings prepared from the 0.125 M precursor solution, the volume sprayed (20 ml) was twice the volume sprayed (10 ml) for the coatings prepared from the 0.25 M precursor solution. Hence, approximately the same amount of products was deposited for both coatings. However, the volume flow was kept constant for both precursor

solutions and consequently the deposition rate was doubled for the 0.25 M precursor solution. This indicates that the coatings prepared from the 0.125 M precursor solution with a volume of 20 ml had more time to evaporate and partially decompose at the substrate before a new layer of products was deposited. For the coatings prepared from the 0.25 M precursor solution with a volume of 10 ml, the deposition rate was higher giving less time for reactions on the substrate. Therefore, a higher temperature was needed to deposit crack-free green coatings for coatings prepared from 10 ml of the 0.25 M precursor solution compared to the coatings prepared from 20 ml of the 0.125 M precursor solution.

TG and FTIR confirmed the presence of nitrate species in the coatings and therefore the deposition of droplets or ionic salt precipitates on the substrate. The observed band of O-H and H_2O in FTIR and the mass loss around 100 °C in TGA can be explained by either the presence of solvent in the film or the absorption of water molecules by the nitrate species.

The first derivative of the mass as a function of temperature is shown for coating 8YSZ(0.125)-750-20-ND in Figure 5.2. The first derivatives are plotted individually for coatings 8YSZ(0.125)-650-20-ND, 8YSZ(0.125)-700-20-ND and 8YSZ(0.25)-700-10-ND in respectively Figure B.4, Figure B.5 and Figure B.6 in Appendix B. By use of the first derivative, estimates of mass loss attributed to nitrates could be found as illustrated in Figure 5.2. The mass losses attributed to nitrates were estimated to be 22 and 24 % for respectively the “high temperature coatings” and the “low temperature coatings”. This is in good agreement with Figure 4.10 showing that the mass loss attributed to nitrate decomposition was less for the “high temperature coatings” compared to the “low temperature structures”. These observations indicate that for the “high temperature coatings” partial nitrate decomposition took place in the latest stage of the deposition.

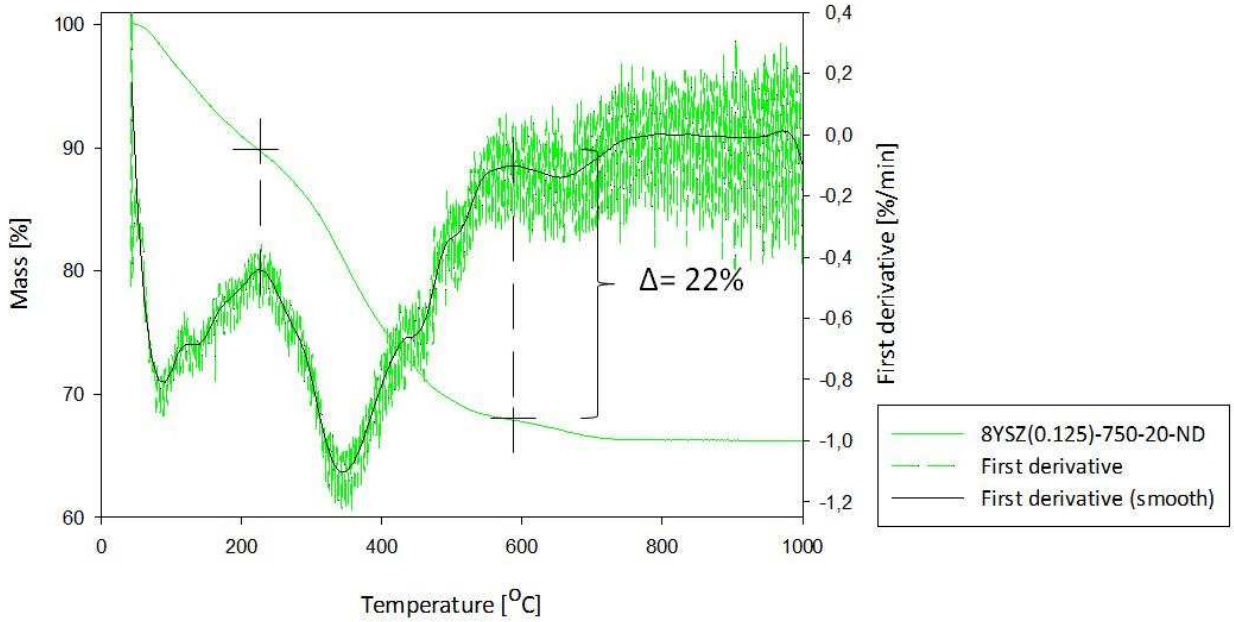

Figure 5.2: TGA of coating 8YSZ(0.125)-750-20-ND. Included in the figure is the first derivative of the mass as a function of temperature.

5.2.4 Microstructure

The delamination of coatings sprayed without drying is believed to be caused by the nitrates being highly hygroscopic. When the nitrates absorbs water after deposition, which was lost during deposition, the volume of the deposited film increases and the film delaminates to release the associated stresses. This volume increase is also believed to be the reason why the density of cracks increased one day after spray pyrolysis as shown for coating 8YSZ(0.125)-700-20-ND in Figure 4.7b and Figure 4.14b.

Due to the fact that a TBC is an insulation layer, a temperature gradient is expected throughout the coating thickness. The part of the coating nearest the interface between the coating and the substrate are exposed to a higher temperature for a longer period of time compared to the coating at the surface during deposition. Due to the temperature gradient and the deposition time, the microstructure can differ from the surface to the interface surface between the substrate and the coating. However, no distinct difference was observed between the microstructure observed from above and from beneath for coating 8YSZ(0.25)-700-10-ND and 8YSZ(0.125)-700-20-ND, which is believed to be related to the low thickness of the coatings.

The ageing phenomenon, where segregation led to one zirconium rich phase and one yttrium rich phase, observed for coating 8YSZ(0.25)-700-10-ND one day after spraying, was probably attributed to the presence of solvent in the coating after deposition. The same phenomenon was not observed for coating 8YSZ(0.125)-700-20-ND one day after spraying indicating that the solvent evaporated during transport to the substrate, resulting in an ionic salt precipitate deposition with a more homogenous mixing of the different cations.

5.2.5 Heat Treatment

After deposition, the coatings have an amorphous structure with a broad peak slightly below 2θ=30° as shown in Figure 4.16. This angle is in the area where the largest intensity diffraction line for the cubic, tetragonal and monoclinic phase of YSZ appears. The sharp peak at about 2θ=50° is attributed to the stainless steel substrate. As a consequence, further heat treatment is required to crystallize the YSZ coatings.

When the set-point temperature was fixed to 700 °C, sprayed coatings dried on the heating plate with or without gas supply were exposed to respectively 190 and 440 °C during drying, temperatures at which nitrate decomposition is expected that may lead to cracks in the coatings. When comparing the structures in Figure 4.17b and c, it can be seen that by increasing the drying time, the density and size of the cracks increase. Comparing the structures in Figure 4.17a and b, it shows that during drying, the size of the cracks seems to increase with increasing substrate temperature.

After heat treatment in the furnace at 600 °C with a slow heating rate, the crack size has increased for coating 8YSZ(0.25)-700-10-SH compared to coating 8YSZ(0.25)-700-10-15min^{-}, while coating 8YSZ(0.125)-700-20-SH delaminated from the substrate in some areas. It is believed that the long drying time could be the reason for the increased cracking and delamination.

As described in Section 2.6.2, for TBCs made by spray pyrolysis of an aqueous nitrate precursor solution, the vertical cracks should not be introduced into the coating during deposition, but during the decomposition of the nitrates after spray pyrolysis. For coating 8YSZ(0.125)-700-20-ND, the heat treatment has shown the possibility of introducing vertical cracks into the coating during decomposition. As shown in Figure 4.18 and Figure 4.19, by changing the drying times and conditions, it is possible to tailor the crack propagation to get the preferred size and geometry of the cracks.

5.2.6 Multi-Layered Coatings

The thickness of a ceramic top coat is normally in the range of 100 to 400 µm [1]. As discussed in Section 5.2.2, the coating thickness is limited to a maximum thickness before cracking and delamination during deposition. However, spraying multiple thin layers gives the opportunity to increase the total coating thickness.

Coatings 8YSZ(0.125)-700-2x20-2x5min^{+} and 8YSZ(0.125)-700-2x20-2x5min^{-} were still continuous and had good adhesion to the substrate after the second layer was deposited. After deposition of the second layer the homogeneity of the coatings seemed to increase compared to coatings 8YSZ(0.125)-700-20-5min^{+} and 8YSZ(0.125)-700-20-5min^{-}. The deposition of a second layer showed that it was possible to double the thickness of the single-layered coating. In addition to the higher thickness and good adhesion to the substrate after deposition, the

good homogeneity between the two layers supported the feasibility of depositing multiple layers by spray pyrolysis to increase the thickness. However, the method needs to be further optimized to achieve even higher thicknesses.

6 Conclusions and Further Work

8YSZ coatings have been deposited on stainless steel substrates by spray pyrolysis of an aqueous nitrate precursor solution. The precursor solution concentration and deposition parameters, including set-point temperature and volume sprayed, were optimized for 8YSZ to produce continuous and crack-free green coatings.

The influence of the substrate temperature on the microstructure of the deposited green coatings was investigated. A substantial change in microstructure was observed for the green coatings prepared from the 0.25 M precursor solution between set-point temperatures of 700-725 °C, and for the green coatings prepared from the 0.125 M precursor solution between set-point temperatures of 650-200 °C. Reasons for the structure changes were suggested based on characterization of the deposited green coatings with regards to microstructure, composition and thickness. For the inhomogeneous and cracked “low temperature structure”, the temperature was below the minimum deposition temperature needed to achieve crack-free green coatings. The evaporation of the solvent still present in the deposited film resulted in severe cracking of the film. For the thinner, more homogenous and almost crack-free “high temperature coatings”, the temperature was within the temperature interval for crack-free green coating deposition. The solvent evaporated during droplet transport and ionic salt precipitates were deposited on the substrate.

Vertical cracks, known to be beneficial for TBCs, were introduced into the crack-free green coatings during nitrate decomposition. The cracking behavior of the coatings was investigated for different drying times and conditions, in order to tailor the crack propagation to obtain narrow vertical cracks. During drying on the heating plate, the density and size of the cracks increased with both increasing substrate temperature and drying time.

A higher temperature was needed to deposit crack-free green coatings from 10 ml of the 0.25 M precursor solution compared to 20 ml of the 0.125 M precursor solution. Since the volume flow was kept constant for both precursor solutions, the deposition rate was doubled for the 0.25 M precursor solution giving a higher deposition rate and less time for reactions in the deposited film. Consequently, a higher temperature was necessary to deposit crack-free green coatings.

For a given precursor solution concentration, it was found that there was a maximum film thickness achieved before spallation of the coating occurred due to built-up stresses which exceed the fracture toughness of the material. Increasing the precursor solution concentration consequently requires a decrease in the sprayed volume during spray pyrolysis. However, decreasing the deposited volume resulted in a decrease in coating thickness.

The thicknesses of the green coatings were found to be in the range 10-20 µm. As this thickness is lower than the thickness required for a TBC, the possibility of spraying multi-layered coatings was investigated. Two different two-layered coatings were prepared. After deposition of the

second layer the coatings still had good adhesion to the substrate and it was not possible to distinguish between the two layers. Introducing a second layer also showed that it was possible to double the thickness of the single-layered coating, demonstrating the feasibility of depositing multiple layers by spray pyrolysis to increase the thickness. However, the method needs to be further optimized to achieve even higher thicknesses.

The work described in this thesis has demonstrated the possibility to tailor the crack propagation in order to get the preferred size and geometry of the cracks for one-layered coatings. However, the cracking behavior of a multi-layered coating is more complex and needs to be further investigated. It is therefore important to find a suitable method for more extensive cross-section examinations in order to study both the homogeneity between the different layers, and the vertical crack distribution in each layer in more detail.

Even though successful coatings of 8YSZ have been prepared during the work described in this thesis, further coating characterization with regards to thermal conductivity, thermal stability, hardness, roughness and wear resistance is necessary to investigate the possibility of using 8YSZ coatings prepared by spray pyrolysis as TBCs.

7 References

1. N.P. Padture, M. Gell and E.H. Jordan, *Thermal Barrier Coatings for Gas-Turbine Engine Applications.* Science, 2002. **296**: p. 280-284.
2. A. Feuerstein, J. Knapp, T. Taylor, A. Ashary, A. Bolcavage and N. Hitchman, *Technical and Economical Aspects of Current Thermal Barrier Coating Systems for Gas Turbine Engines by Thermal Spray and EBPVD: A Review.* Journal of Thermal Spray Technology, 2008. **17**(2): p. 199-213.
3. D. W.Richerson, *Modern Ceramic Engineering Properties, Processing, and use in Design*. 3 ed. 2006: Taylor & Francis group.
4. X.Q. Cao, R. Vassen and D. Stoever, *Ceramic materials for thermal barrier coatings.* Journal of the European Ceramic Society, 2004. **24**(1): p. 1-10.
5. I. Askestad, *Ceramic Thermal Barrier Coatings*. 2010, Norwegian University of Science and Technology: Trondheim.
6. M. Gell, E.H. Jordan, M. Teicholz, B.M. Cetengen, N.P. Padture, L. Xie, D. Chen, X. Ma and J. Roth, *Thermal Barrier Coatings Made by the Solution Precursor Plasma Spray Process.* Journal of Thermal Spray Technology, 2007. **17**(1): p. 124-135.
7. L. Xie, D. Chen, E.H. Jordan, A. Ozturk, F. Wu, X. Ma, B.M. Cetegen and M. Gell, *Formation of vertical cracks in solution-precursor plasma-sprayed thermal barrier coatings.* Surface and Coatings Technology, 2006. **201**(3-4): p. 1058-1064.
8. S. Weber, H.L. Lein, T. Grande and M.A. Einarsrud, *Deposition of Thick Coatings by Spray Pyrolysis.* 2011.
9. N. Birks, G.H. Meier and F.S. Pettit, *Protective Coatings*, in *Introduction to the High-Temperature Oxidation of Metals*.
10. *Thermal barrier coatings*. [cited 2010 5.september]; Available from: http://www.ipm.virginia.edu/research/PVD/Pubs/thesis6/chapter2.PDF.
11. Ashwin. *Seminar topic: thermal barrier coatings*. [cited 2010 29.september]; Available from: http://seminartopic4all.blogspot.com/.
12. *Thermal barrier coating*. [cited 2010 5.september]; Available from: http://en.wikipedia.org/wiki/Thermal_barrier_coating.
13. *How gas turbine engines work*. [cited 2010 5.september]; Available from: http://science.howstuffworks.com/transport/flight/modern/turbine.htm.
14. *Coating for high temperature applications*. [cited 2010 5.september]; Available from: http://www.thomas-sourmail.org/coatings/single-page.html.
15. B. Sundhangshu, *High Temperature Coatings*. 2007, USA: Butterworth-Heinemann.
16. P.I. Dahl, *Synthesis and Characterization of Ionic Conductors based on ZrO_2, $BaZrO_3$ and $SrCeO_3$ and Preparation of $LaFeO_3$ and $LaCoO_3$ thin films*, in *Materials Science and Engineering* 2006, Norwegian Univeristy of Sience and Technology: Trondheim.
17. V.S Stubican, R.C.Hink and S.P.Ray, *Phase Equilibria and Ordering in the System ZrO_2-Y_2O_3.* Journal of the American Ceramic Society, 1978. **61**(1-2): p. 17-21.

18. P. Atkins, T. Overton, J. Rourke, M. Weller and F. Armstrong, *Shriver and Atkins, Inorganic Chemistry*. Fourth ed. 2006: Oxford.
19. D.L. Clark. *SSRL Studies Aid Environmental Cleanup at Rocky Flats*. [cited 2011 7 february]; Available from: http://ssrl.slac.stanford.edu/research/highlights_archive/rockyflats.html.
20. J.D. McCullough and K.N. Trueblood, *The Crystal Structure of Baddeleyite (monoclinic ZrO_2).* Acta Crystallographica, 1959. **12**: p. 507.
21. G. Teufer, *The crystal structure of tetragonal ZrO_2.* Acta Crystallographica, 1962. **15**: p. 1187.
22. R.J.D. Tilley, *Understanding solids: The science of materials*. 2008: John Wiley & Sons Ltd.
23. H. Zhou, F. Li, B. He, J. Wang and B.-d. Sun, *Air plasma sprayed thermal barrier coatings on titanium alloy substrates.* Surface and Coatings Technology, 2007. **201**(16-17): p. 7360-7367.
24. J. Nair, P. Nair, G.B.M. Doesburg, J.G. Van Ommen, J.R.H. Ross, A.J. Burggraaf and F. Mizukami, *Sintering of lanthanum zirconate.* Journal of the American Ceramic Society, 1999. **82**(8): p. 2066-2072.
25. B. Liu, J.Y. Wang, Y.C. Zhou, T. Liao and F.Z. Li, *Theoretical elastic stiffness, structure stability and thermal conductivity of La2Zr2O7 pyrochlore.* Acta Materialia, 2007. **55**(9): p. 2949-2957.
26. *Crystallographic Data for $La_2Zr_2O_7$*. 2010, Springer Materials.
27. H. Zhou, D. Yi, Z. Yu and L. Xiao, *Preparation and thermophysical properties of CeO_2 doped $La_2Zr_2O_7$ ceramic for thermal barrier coatings.* Journal of Alloys and Compounds, 2006. **438**: p. 217-221.
28. D. Perepdnis and L. J.Gauckler, *Thin Film Deposition Using Spray Pyrolysis.* Journal of Electroceramics, 2005. **14**: p. 103-111.
29. *Stainless Steel Balls, Inox Steel Ball* [cited 2010 17.december]; Available from: http://www.steelmedia.com/stainless-steel-balls.htm.
30. S. Weber. 2010: Trondheim.
31. D.W. Mayo, F.A. Miller and R.W. Hannah, *Course Notes On the Interpretation of Infrared and Raman Spectra*. 2003, Wiley & Sons, Inc.
32. E.D. Ion, B. Malic, I. Arcon, J.P. Gomilsek, A. Kodre and M. Kosec, *Characterization of lanthanum zirconate prepared by a nitrate-modified alkoxide synthesis route: From sol to crystalline powder.* Journal of the European Ceramic Society, 2010. **30**(2): p. 569-575.
33. T. Mokkelbost, I. Kaus, T. Grande and M.A. Einarsrud, *Combustion Synthesis and Characterization of Nanocrystalline CeO_2-Based Powders.* American Chemical Society, 2004.

Appendix A: Powder Characterization

The diffractograms in Figure A.1, Figure A.2, Figure A.3 and Figure A.4 presents XRD results of respectively 8YSZ, 4YSZ, 3YSZ and 1.5YSZ powders calcined at 1100 °C for 2 hours. The diffraction lines associated with the different phases are included in the figures. For 8YSZ powder, the cubic phase was stabilized. For 4YSZ, 3YSZ and 1.5YSZ powder, both tetragonal and monoclinic phases were present.

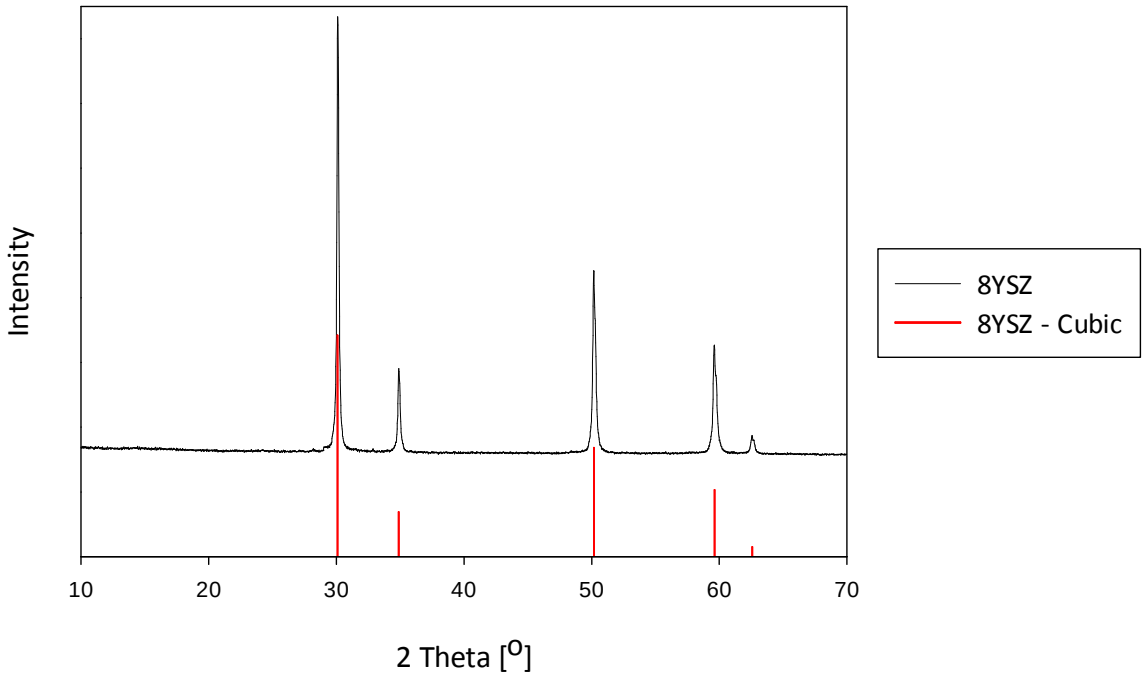

Figure A.1: XRD diffractogram of 8YSZ powder calcined at 1100 °C for 2 hours. The diffraction lines included in the figure shows that the cubic phase of 8YSZ was stabilized.

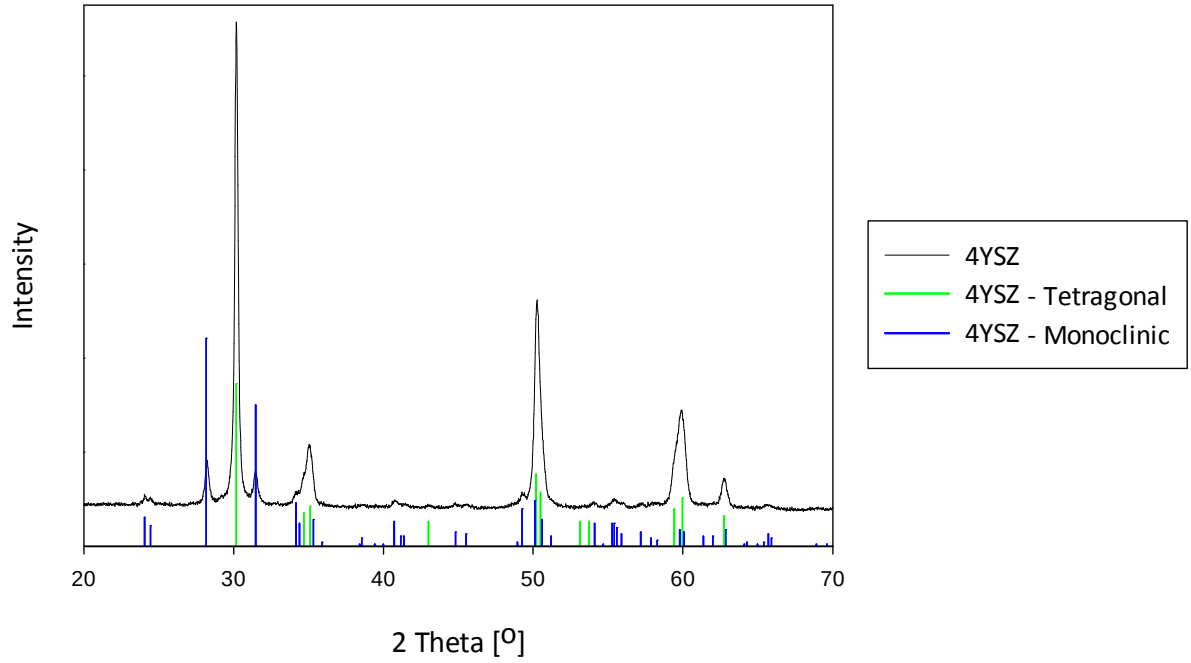

Figure A.2: XRD diffractogram of 4YSZ powder calcined at 1100 °C for 2 hours. The diffraction lines included in the figure show that the tetragonal structure of 4YSZ was the dominating phase. A small amount of the monoclinic structure was also present.

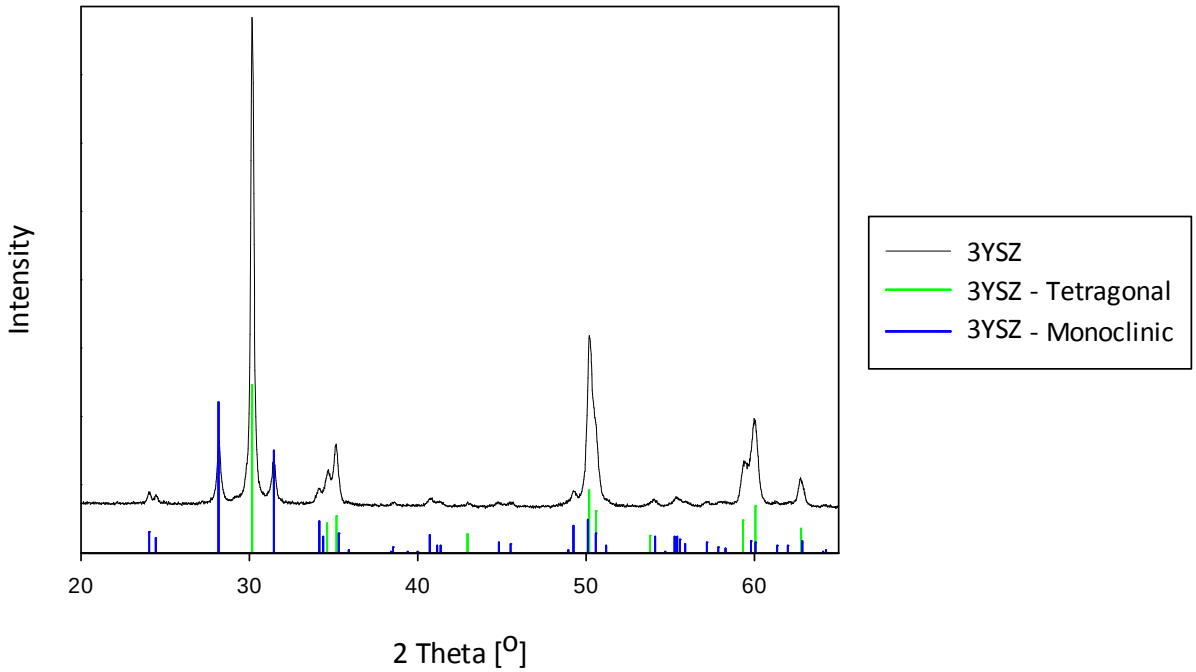

Figure A.3: XRD diffractogram of 3YSZ powder calcined at 1100 °C for 2 hours. The diffraction lines included in the figure show that the tetragonal structure of 3YSZ was the dominating phase. A small amount of the monoclinic structure was also present.

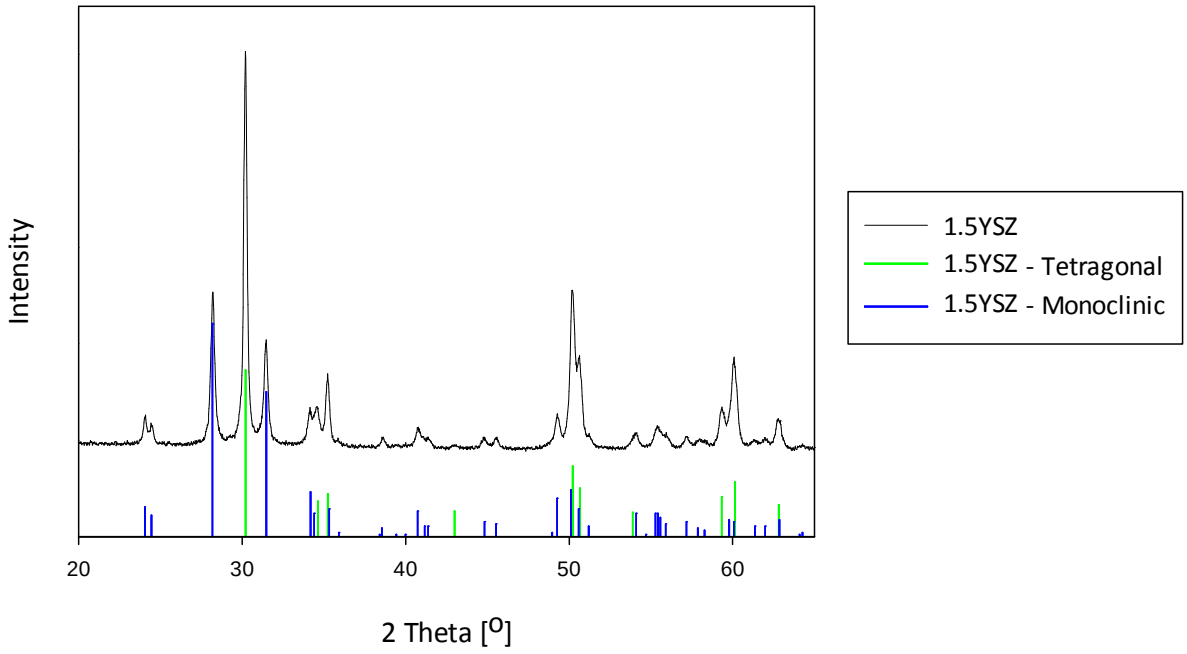

Figure A.4: XRD diffractogram of 1.5YSZ powder calcined at 1100 °C for 2 hours. The diffraction lines included in the figure show that both the tetragonal and the monoclinic structures of YSZ were present.

Appendix B: TG and FTIR

Figure B.1, Figure B.2 and Figure B.3 present FTIR spectra of coatings 8YSZ(0.125)-700-20-ND, 8YSZ(0.125)-750-20-ND and 8YSZ(0.25)-700-10-ND respectively.

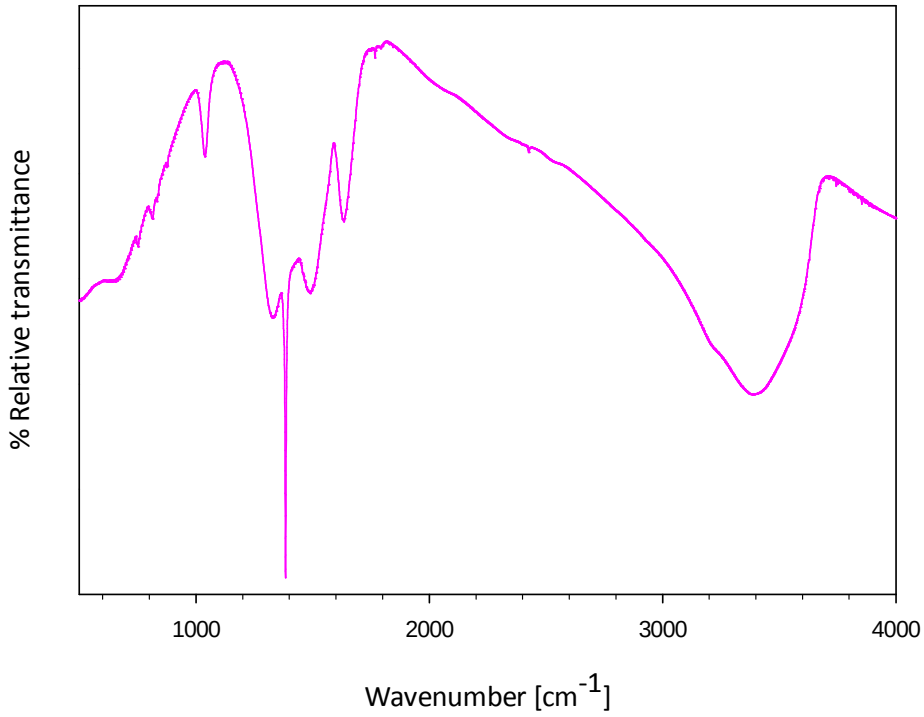

Figure B.1: FTIR spectrum of coating 8YSZ(0.125)-700-20-ND.

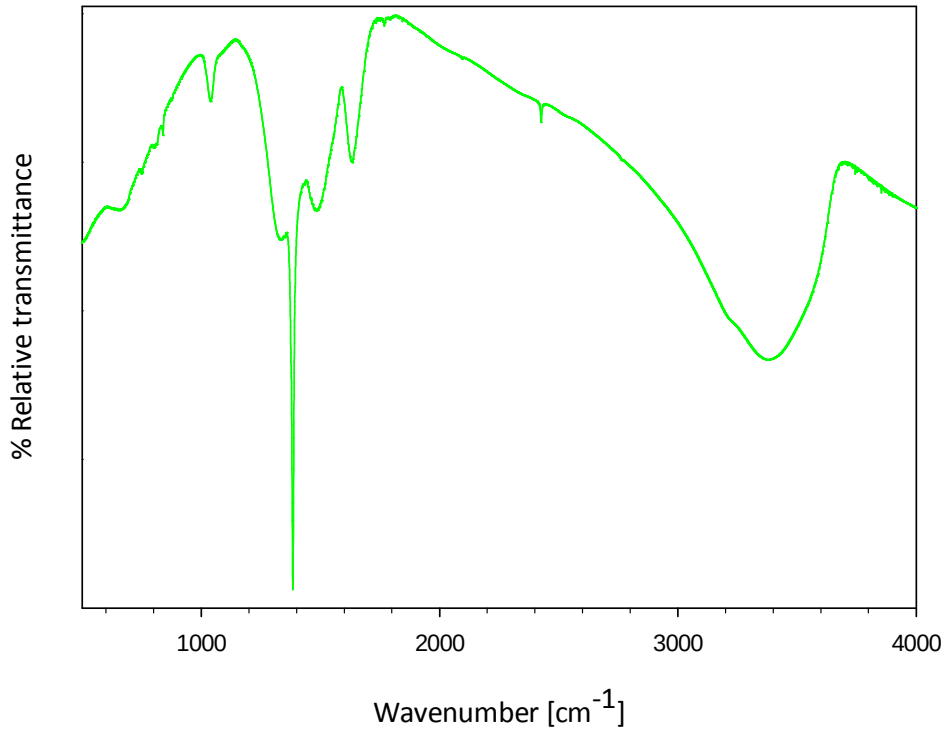

Figure B.2: FTIR spectrum of coating 8YSZ(0.125)-750-20-ND.

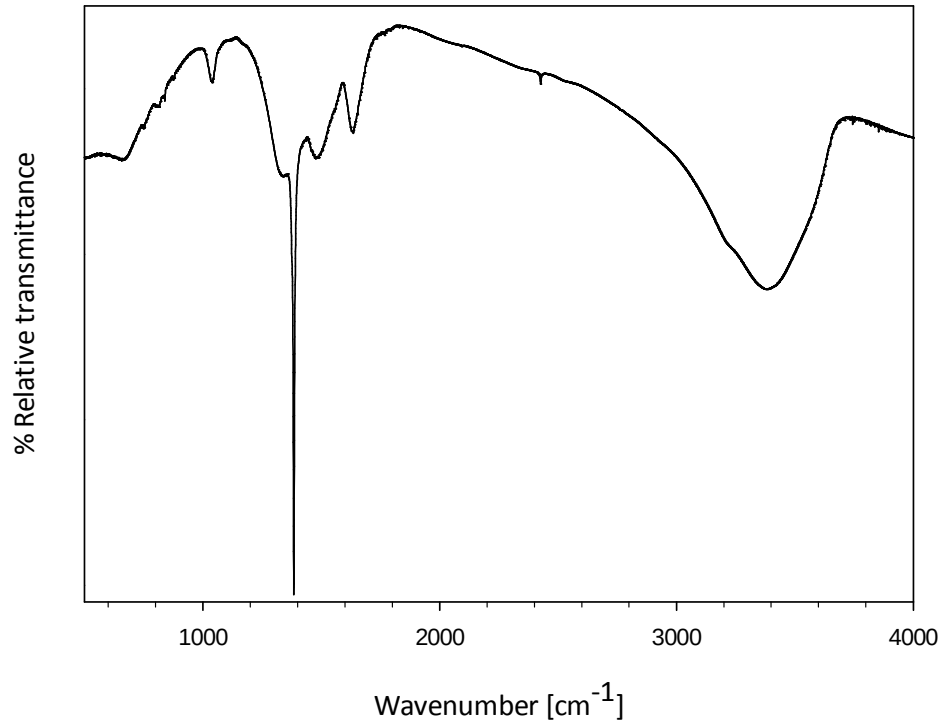

Figure B.3: FTIR spectrum of coating 8YSZ(0.25)-700-10-ND.

Figure B.4, Figure B.5 and Figure B.6 present thermogravimetric analysis of coatings 8YSZ(0.125)-650-20-ND, 8YSZ(0.125)-700-20-ND and 8YSZ(0.25)-700-10-ND respectively. Included in the figures are plots of the first derivative of the mass as a function of temperature.

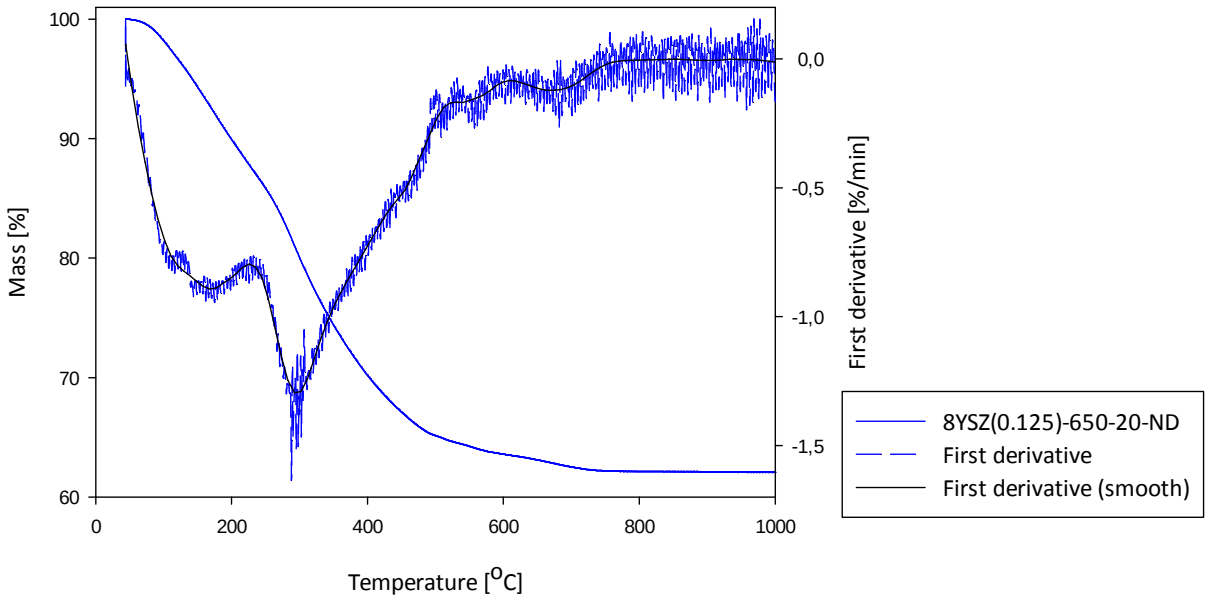

Figure B.4: TGA of coating 8YSZ(0.125)-650-20-ND. Included in the figure is the first derivative of the mass as a function of temperature.

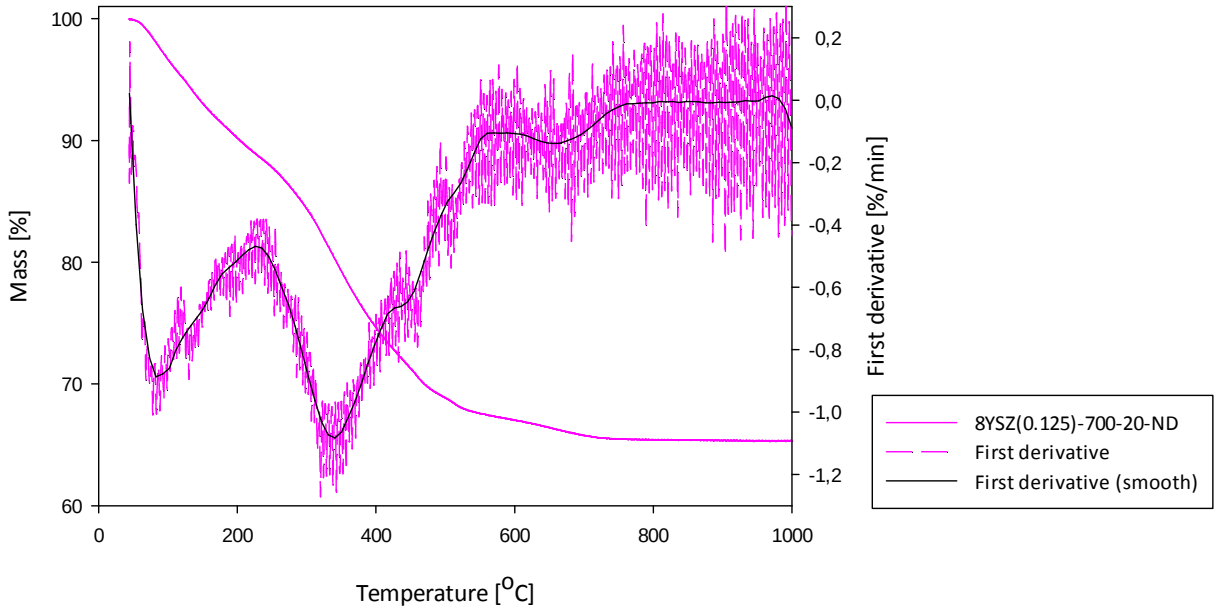

Figure B.5: TGA of coating 8YSZ(0.125)-700-20-ND. Included in the figure is the first derivative of the mass as a function of temperature.

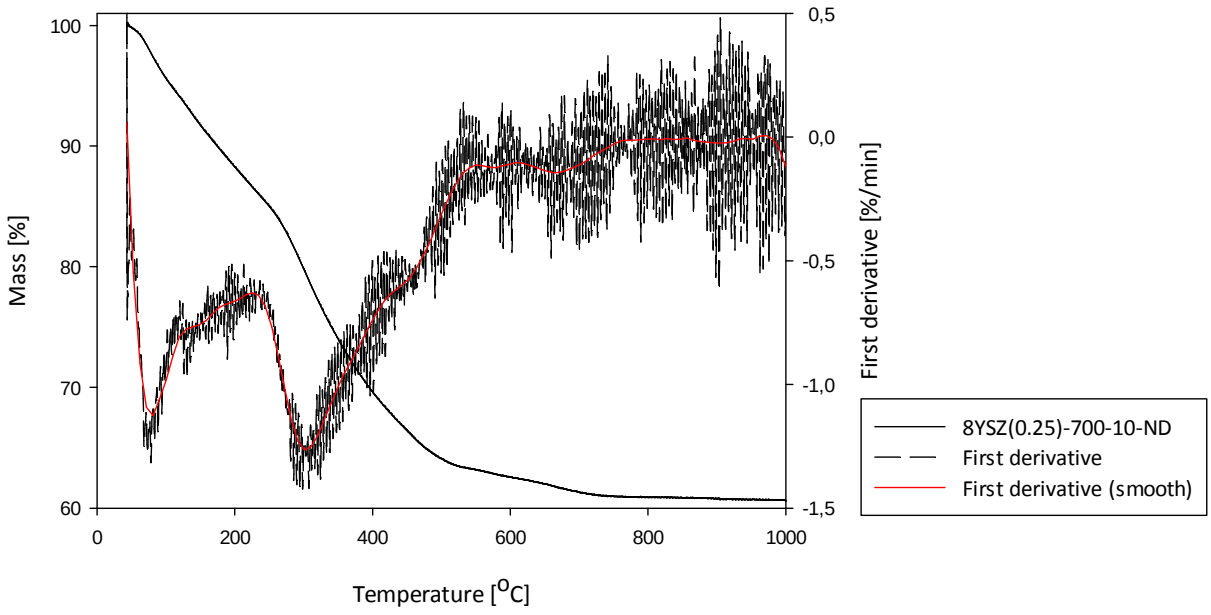

Figure B.6: TGA of coating 8YSZ(0.25)-700-10-ND. Included in the figure is the first derivative of the mass as a function of temperature.